Chapter 18. Stable isotope paleoecology of the late Miocene Baynunah Formation, Abu Dhabi, United Arab Emirates

Kevin T. Uno[1] and Faysal Bibi[2]

Author affiliations:

1) Division of Biology and Paleo Environment, Lamont-Doherty Earth Observatory of Columbia University, Palisades, New York, 10964 USA
2) Museum für Naturkunde, Leibniz Institute for Evolution and Biodiversity Science, Invalidenstrasse 43, 10115 Berlin, Germany

Author email addresses:

kevinuno@ldeo.columbia.edu , faysal.bibi@mfn.berlin

Abstract

The Baynunah Formation contains the only known late Miocene terrestrial fossils from the Arabian Peninsula. Based on renewed field work since 2002, we present paleoenvironmental and dietary reconstructions from carbon isotope data from plant wax biomarkers and carbon and oxygen isotope data from fossil tooth enamel in combination with previously published fossil tooth enamel and pedogenic carbonate isotope data. The organic and isotopic data indicate that the highly seasonal ecosystem supported a herbivore community that relied heavily on C_4 vegetation. Carbon isotope and molecular abundance data from *n*-alkanes indicate mostly mixed C_3-C_4 and C_4-dominated ecosystems. Carbon isotope data from fossil teeth indicate a range of C_3, mixed C_3-C_4, and C_4 diets, with suids, deinotherids, and rhinocerotids browsing, and bovids, elephantids, and equids mixed feeding to grazing. Hippopotamids show the most positive carbon and most negative oxygen values, with narrow ranges indicating year-round grazing and semi-aquatic habits. The Baynunah sivatheres represents the earliest evidence for a C_4-dominanted diet in the giraffids. Equid intratooth oxygen isotope profiles indicate a highly seasonal hydroclimate regime, reflecting strong monsoonal conditions with a single rainy season. Corresponding carbon profiles record large seasonal changes in equid diets, with mainly grazing in the wet season and greater ingestion of browse in the dry season. Baynunah ecosystems comprised savanna habitats (woody grasslands) with the proboscidean trackway site of Mleisa 1 likely being a seasonally flooded C_4 grassland.

1. Introduction

The Baynunah Formation contains the only known terrestrial vertebrate fossils from the late Miocene of the Arabian Peninsula. Nearly all outcrops of the Baynunah Formation are jebels, poking out of the sea of sands in western Abu Dhabi Emirate (Fig. 18.1). The formation is several tens of meters thick in most places and exceeds 50 m at the type section at Jebel Barakah (Whybrow et al., 1999). The lower part of the formation is comprised primarily of fossil bearing fluvial channel deposits and paleosols, whereas the upper part has some carbonate beds and several packages of finer grained sediments that suggest small lakes or seasonally flooded areas (fig. 3.2, Schuster, this volume). Channel clasts in the lower part of the formation are commonly reworked, intraformational pedogenic carbonates or rarely, oncolites. Root casts are a common feature of the paleosols and sandy channel deposits. More detailed descriptions of the sedimentology, fluvial architecture, and depositional environments are found in the first Baynunah volume (Friend, 1999; Whybrow et al., 1999) and an updated synthesis with new observations is given in Schuster (this volume).

Like much of the Arabian Peninsula, the climate of Abu Dhabi is hyperarid, with mean annual temperature in excess of 27 °C and annual precipitation of less than 100 mm per year. The harsh environment today is a stark contrast to what the Baynunah fossil and sedimentary evidence indicates: lush, verdant habitats supported by a perennial braided river system that was home to many large mammals, including ancestral elephants, horses, hippos, antelopes, giraffes, rhinos, and pigs, among other mammals, reptiles, fishes, birds, and invertebrates (Whybrow and Hill, 1999 and Ch. 6-16, this volume).

FIG. 18.1 NEAR HERE. Width = 1.5 columns.

The fossils of the Baynunah Formation were likely known to locals for centuries, but the first written records in English come from petroleum industry reports from the late 1940s and early 1950s (Hill et al., 1999; Bibi, Ch. 2, this volume). These early reports eventually led to a collaborative research project on the geology and fauna of the Baynunah Formation in the 1980s-1990s, which culminated in the publication of the first research volume (Whybrow and Hill, 1999). Fieldwork in the Baynunah Formation resumed in 2002 and a wealth of new fossil material has been recovered since then. The amount of new fossil material and sites warrants a fresh look at the Baynunah material and its paleoecological context. Also, since 1999, many new records have been published that document regional vegetation, dietary, and faunal change across Neogene sites of the Old World (Badgley et al., 2008; Barry et al., 2002; Behrensmeyer et al., 2007; Feakins et al., 2005; Leakey and Harris, 2003; Polissar et al., 2019; Uno et al., 2011; Uno et al., 2016a). The paleoecology of Baynunah has therefore much to contribute to the global context of late Neogene ecosystem change, characterized by the expansion of C_4 grasslands and mammalian dietary shifts. Furthermore, new analytical techniques, such as compound specific isotope analysis of plant waxes, are now available and can contribute additional information on this site. Stable isotope analyses of biomarkers (plant waxes) and biominerals (tooth enamel) are now well-established and widely used methods to reconstruct mammal diets and terrestrial vegetation.

In this chapter, we use geochemical analyses of plant wax biomarkers and fossil tooth enamel to reconstruct the vegetation, hydroclimate, and mammalian diets of the Baynunah

Formation. Carbon isotope ratios of plant wax biomarkers extracted from sediments are used to reconstruct the proportion of C_3 to C_4 vegetation. We reconstruct the diets of eight herbivore lineages using carbon isotope ratios in fossil tooth enamel and evaluate the dietary structure of the herbivore community. Oxygen isotope ratios in tooth enamel provide additional information on the dietary niche partitioning and environmental aridity. We assess the seasonality of vegetation, precipitation, and equid diets from intratooth isotope profiles of their cheek teeth. Environmental and dietary reconstructions incorporate previously published stable isotope data from pedogenic carbonate and fossil tooth enamel data from Kingston (1999). Together, these data support previous interpretations and also give new insight into the paleoecology of the Baynunah. To provide a more global perspective, we compare the Baynunah tooth enamel and pedogenic carbonate isotope data to isotope data from other major late Miocene fossil localities in Africa and South Asia.

2. Materials and Methods

2.1. Materials

The material used in this study includes fossil teeth that were sampled in 2011 and 2014. Baynunah Formation sediments analyzed for compound specific carbon isotope ratios of plant waxes were collected in December 2014. All fossil localities are described in detail in Chapter 2 (Bibi et al.). Sampled sites are shown in Fig. 18.1.

We also consider the tooth enamel and pedogenic carbonate isotope data presented by Kingston (1999). Some of the fossil enamel samples are not associated with a specimen number – these are identified only by his 'AD' numbering system (not to be confused with cataloged

specimen numbers, which begin with AUH). Some of the enamel and most of his paleosol samples are from unknown localities within site areas, and these are denoted here by "UL".

Sediments for plant wax analyses were collected from fine grained deposits, typically brown or green silts or silty clays at Hamra (HMR 5), Ruwais (RUW SE), Kihal (KIH 1, UL), and Mleisa (MLS 1) (Fig. 18.1). Fossil teeth come from surface and *in situ* finds at Jebel Barakah (JBR UL), Shuwaihat (SHU 1, 2, and 4), HMR (1, 2 , 3, 5 and 6), Jebel Dhanna (JDH 4), Ras Dubay'ah (RDB 2 and UL), Jebel Mimiyah (MIM 1), Ruwais (RUW UL), and Gerain al Aysh (GAA 1, 2, and 3). Additionally, we discuss tooth enamel data from HMR (1, 5, and UL), JBR (2 and 'east'), JDH (3, 4, 5, and UL), KIH (1 and UL), RDB 2, SHU (1 and 4), and THM 4, and pedogenic carbonate data from JBR 2, 3, and UL ('JB20'), SHU UL ('S8'), HMR UL ('HMR12–16'), and KIH UL ('K4 and 5'), previously published by Kingston (1999).

Given the patchy exposure of the Baynunah Formation, the broadly similar depositional environments present across the localities, and the limited thickness of the formation that suggests a geologically brief deposition interval (perhaps 100–200 ka, see Bibi et al., Ch. 19 and Peppe, Ch 4., this volume), the ages of all tooth enamel and plant wax samples from the Baynunah fossil localities are considered to be broadly contemporaneous.

2.2. Methods

2.2.1. Stable isotopes in vegetation and teeth

In tropical and subtropical ecosystems today, woody plants use the C_3 photosynthetic pathway, or Calvin cycle, while low elevation (<1500 m) grasses, some sedges (e.g., *Cyperus papyrus*), and select shrubs (e.g., *Salsola* sp.) use the C_4 pathway, or Hatch-Slack cycle (Cerling

and Harris, 1999; Livingstone and Clayton, 1980; Tieszen et al., 1979; Young and Young, 1983).

The carbon isotope ratio of C_3 plants today is around −28 ‰ on average with an observed range of about −36 to −23 ‰. The wide range in $\delta^{13}C$ values in the bulk tissues of C_3 plants is controlled by environmental conditions: more negative values are found in closed canopy forests whereas xeric conditions—common across the Arabian Peninsula today—lead to more positive values (e.g., −26 to −23 ‰). C_4 plants exhibit a narrower range of values, from about −14 to −10 ‰ (Cerling et al., 2003b). Stable carbon and oxygen isotope ratios are reported as delta (δ) values relative to the Pee Dee Belemnite (PDB) standard using permil (‰) notation where

$$\delta^{13}C \text{ (or } \delta^{18}O) = (R_{sample}/ R_{standard} - 1) \times 1000 \quad (1)$$

and R_{sample} and $R_{standard}$ are the $^{13}C/^{12}C$ ($^{18}O/^{16}O$) ratios in the sample and in the standard, respectively, and the $\delta^{13}C$ and $\delta^{18}O$ values of PDB are defined as 0‰.

Terrestrial plants produce long chain *n*-alkyl lipids primarily as epicuticular waxes on their leaves (Eglinton and Hamilton, 1967). The two types of *n*-alkyl lipids analyzed in this study are *n*-alkanes, which are linear, saturated hydrocarbon molecules, and *n*-alkanoic acids, which are similar in structure to *n*-alkanes but have a terminal carboxyl group. *n*-Alkanoic acids are commonly referred to as fatty acids. Due to their structure, *n*-alkanes and fatty acids are recalcitrant and resistant to microbial breakdown, and are therefore commonly preserved in fluvio-lacustrine sediments over millions of years (Uno et al., 2016b). While there are a variety of *n*-alkyl lipid sources in sediments, terrestrial plants produce long chain homologs, generally those with ≥26 carbon chainlengths. Whereas, short chain *n*-alkyl lipids (C_8 to C_{18}) are produced by bacteria or microbes and mid-chain lipids (C_{19} to C_{25}) can also be microbial in origin or come from aquatic macrophytes or sphagnum (Corrigan et al., 1973; Cranwell et al., 1987; Ficken et

al., 2000; Nott et al., 2000). In terrestrial plants, odd numbered *n*-alkanes homologs (e.g., C_{27}, C_{29}, and C_{31}) occur in higher concentrations compared to even-numbered ones. The odd-over-even preference in *n*-alkanes provides a unique signature of plant origin. A common measure of this metric is the carbon preference index (CPI), which is calculated using the equation from Marzi et al. (1993) for both *n*-alkanes and fatty acids. The CPI of plants ranges widely, but is generally between 5 and 40 (Bush and McInerney, 2013), and is usually lower, from about 2 to 10, in soils (Bush and McInerney, 2015). Plant-derived fatty acids show a similar pattern, but instead have an even-over-odd preference. Petroleum also consists of *n*-alkanes, but has a CPI of ~1, which allows CPI to be used to verify that *n*-alkyl lipids are from plants rather than petroleum. We also report the average chain length (ACL), which is an abundance weighted average of the area of odd numbered *n*-alkanes homologs (C_{27} to C_{35}) or even numbered fatty acids (C_{26} to C_{34}).

In the early 1990's, Hayes and colleagues developed a method to measure carbon isotope ratios of *n*-alkyl lipids and other molecular biomarkers, paving the way for paleovegetation studies using compound specific isotope analysis of biomarkers (Freeman et al., 1990; Hayes et al., 1990). Carbon isotope measurements of *n*-alkanes from terrestrial sedimentary archives can be used to determine the proportion of C_3 to C_4 plants on the landscape, similar to carbon isotope ratios in soil organic matter (Baczynski et al., 2016; Freeman and Colarusso, 2001; Uno et al., 2016b).

Stable carbon and oxygen isotope ratios of tooth enamel are determined by an animal's diet and body water, respectively, and therefore can be used to reconstruct herbivore diets, vegetation, and local hydroclimate in past ecosystems (Kingston and Harrison, 2007; Levin et

al., 2006; e.g., Uno et al., 2011). Carbon isotopes in enamel from large herbivores reflect the proportion of C_3 to C_4 vegetation in their diet during the time in which the tooth formed. Oxygen isotopes in enamel are primarily determined by the isotope ratio of precipitation but also influenced by food water; plant water; evaporative processes in soils, plants, and water sources; and animal physiology (Kohn et al., 1996; Levin et al., 2006; Luz et al., 1984). Stable carbon and oxygen isotope ratios of tooth enamel are reported as delta (δ) values relative to the Pee Dee Belemnite (PDB) standard using permil (‰) notation given equation 1.

2.2.2. Carbon isotope enrichment in plant waxes and tooth enamel

Carbon isotope fractionation occurs during the synthesis of plant waxes and during tooth enamel formation. Isotope fractionation is expressed using the term alpha (α), and it occurs during biological processes that include but are not limited to diffusion, enzymatic fixation of carbon, synthesis of lipids, and mineralization. The fractionation between two substrates is described by the following equation

$$\alpha_{atm-plant} = \frac{1000 + \delta^{13}C_{atm}}{1000 + \delta^{13}C_{plant}}, \quad \text{(Eq. 2)}$$

where the fractionation between atmospheric and plant bulk tissue carbon ($\alpha_{atm\text{-}plant}$) is a function of the $\delta^{13}C$ values of the atmosphere and plant. Isotopic enrichment (ε) is another term used to describe changes in the $\delta^{13}C$ value between substrates and is related to α through the following equation:

$$\varepsilon_{atm-plant} = \left(\alpha_{atm-plant} - 1\right) \times 1000 \quad \text{(Eq. 3)}$$

The enrichment factors are necessary for deriving endmember values of C_3 and C_4 for bulk plant tissue, biomarkers, and tooth enamel and are therefore reviewed here. Using known enrichment factors (Table 18.1), the C_3 and C_4 endmembers can be calculated as follows by rearranging equations 2 and 3,

$$\delta^{13}C_{plant} = \frac{1000 + \delta^{13}C_{atm}}{\frac{\varepsilon_{atm-plant}}{1000} + 1} - 1000 \quad \text{(Eq. 4)}$$

The carbon isotope enrichment associated with the synthesis of *n*-alkanes by the plant results in $\delta^{13}C$ values more depleted than bulk plant tissue. In this study we use an enrichment factor, denoted as $\varepsilon^*_{lipid\text{-}plant}$, of −8 ‰. This is based on the $^*_{lipid\text{-}plant}$ mean values determined for C_3 and C_4 plants from Collister et al. (1994). We apply the same $\varepsilon^*_{lipid\text{-}plant}$ of −8 ‰ for fatty acids but acknowledge this number is not yet as well constrained as the value for *n*-alkanes.

For tooth enamel, we use an isotopic enrichment between diet and enamel, denoted as $\varepsilon^*_{enamel\text{-}diet}$, of 14.1 ± 0.5 ‰, as determined by Cerling and Harris (1999) for large ungulates. The $\varepsilon^*_{enamel\text{-}diet}$ value in mammals has recently been found to vary with body mass and the degree of methanogenesis in the gut (Tejada-Lara et al., 2018), with medium to large ungulates generally between 13 and 15 ‰. Uncertainties in estimating precise body mass for the Baynunah fauna preclude application of the equations developed by Tejada-Lara and colleagues for determining $\varepsilon^*_{enamel\text{-}diet}$, so here we use a single value of 14.1 ‰.

2.2.3. C_3 and C_4 endmembers from plant waxes and tooth enamel

In addition to enrichment factors, the atmospheric $\delta^{13}C$ value ($\delta^{13}C_{atm}$) must be known or

estimated in order to establish the C_3 and C_4 endmembers for carbon isotope ratios of plant waxes ($\delta^{13}C_{alkane}$, $\delta^{13}C_{acid}$) and tooth enamel ($\delta^{13}C_{enamel}$). We use the mean value of −6.3 ‰ for the $\delta^{13}C_{atm}$ based on the high resolution benthic foraminifera record from 6 to 8 Ma from Tipple et al. (2010). We use this time interval because it best matches the estimated age for the Baynunah Formation (Bibi et al., Ch. 19; Peppe, Ch. 4, this volume). By combining the $\delta^{13}C_{atm}$ and the biosynthetic fractionation factors for C_3 and C_4 plants, the C_3 and C_4 endmember $\delta^{13}C$ values of bulk tissue can be calculated (Table 18.1). By further applying the enrichment values $\varepsilon^*_{lipid\text{-}plant}$ of −8 ‰ and $\varepsilon^*_{enamel\text{-}diet}$ of 14.1 ‰, the C_3 and C_4 endmembers for $\delta^{13}C_{alkane}$ and $\delta^{13}C_{enamel}$ can be determined. This results in endmember $\delta^{13}C_{alkane}$ values of −33.1 ‰ and −18.8 ‰ for C_3 and C_4 vegetation, respectively. Endmember $\delta^{13}C_{enamel}$ are −11.4 ‰ and + 3.2 ‰ for pure C_3 and C_4 diets, respectively. The $\delta^{13}C_{atm}$ value, enrichment factors, and calculated endmember values are presented in Table 18.1.

With endmember values established, two-member mixing models can be used to estimate the proportion of C_4 vegetation on the landscape or in mammalian diets using $\delta^{13}C_{alkane}$ and $\delta^{13}C_{enamel}$ values, respectively. For plant waxes, we convert only the $\delta^{13}C_{alkane}$ values percent C_4 (%C4) because the carbon isotope systematics of *n*-alkanes are better constrained than for acids using the following equation,

$$\%C4 = \frac{\left(\delta^{13}C_{C3} - \delta^{13}C_{alkane}\right)}{\left(\delta^{13}C_{C3} - \delta^{13}C_{C4}\right)} \times 100 \quad (5)$$

where $\delta^{13}C_{alkane}$ is the measured $\delta^{13}C$ value of the sample and $\delta^{13}C_{C3}$ and $\delta^{13}C_{C4}$ are the calculated C_3 and C_4 endmember values for *n*-alkanes. We propagate the uncertainty in both the *n*-alkane endmember values and in the analytical procedure (± 0.1 ‰), which results in uncertainties of *ca.* 12 to 23 %. We note that uncertainties in the calculated $\%C_4$ are higher towards the C_3 end of the continuum due to the larger uncertainty of the C_3-endmember value, which is ± 4 ‰. We use the same equation (2) to estimate the %C4 in the diet of Baynunah mammals by substituting in the $\delta^{13}C_{enamel}$ for $\delta^{13}C_{alkane}$ and the enamel C_3 and C_4 endmembers (Table 18.1). Using the average C_3 and C_4 $\delta^{13}C_{enamel}$ values we define C_3-dominated diets as those with $\delta^{13}C_{enamel}$ values of ≤ -7.8 ‰ (< 25 $\%C_4$), mixed C_3-C_4 diets as having values from −7.8 to −0.5 ‰ (25-75 $\%C_4$), and C_4-dominated diets as those with $\delta^{13}C_{enamel}$ values of ≥ -0.5 ‰ (>75 $\%C_4$). Finally, we also incorporate into pedogenic carbonate carbon isotope data published by Kingston (1999) into vegetation reconstructions. The $\%C_4$ is similarly calculated from the $\delta^{13}C$ value of the pedogenic carbonate ($\delta^{13}C_{pc}$) using equation 2 and the endmember values given in Table 18.1.

2.2.4. Plant wax sampling and analysis

Approximately 500 g of sediment was collected for plant wax analyses. The sampling protocol was designed to prevent contamination from modern plant biomarkers in the field. Samples were collected by trenching 10 to 80 cm into outcrop surfaces to expose fresh, unweathered sediment. Samples were collected in places where there was little to no overlying modern vegetation and all samples were screened for modern roots, which can be a source of modern *n*alkyl lipids, particularly fatty acids (Mueller et al., 2012). Sediment was collected onto

aluminum foil and the sample collector (K. Uno) wore nitrile gloves to prevent any oils or other foreign lipid sources from contaminating the samples.

In the lab, samples were rinsed with dichloromethane (DCM), an organic solvent, to remove any possible contaminants. A subset of each sample was then crushed to a powder in a mortar and pestle. Lipids were extracted from 103 to 131 g (median: 119 g) of powdered sediment with organic solvents (9:1 DCM : methanol) using a Dionex Accelerated Solvent Extractor in batches of approximately 60 g of sample packed into 66 ml extraction cells. Samples were extracted with four 10 min static cycles at 100° C with a solvent flush volume of 150 % of total cell volume. An internal standard was added to the total lipid extract (TLE) that included 5α-androstane and cis-11-eicosenoic acid (2,000 ng of each) for later quantification of lipids.

The TLE was separated by solid phase extraction on silica gel columns (approx. 0.5 g solvent rinsed silica gel, 230–400 mesh). The aliphatic fraction (F1), which contained *n*-alkanes, was eluted with 4 ml of hexane, the ketone and ester fraction (F2) eluted with 4 ml of DCM, and the polar fraction (F3) with 4 ml of methanol. The F3 fraction was then separated through an aminopropyl column (approx. 0.5g) where the neutral, acid (A) and polar fractions were eluted with 4 ml each of 2:1 DCM:iso-propanol, 4 % acetic acid in diethyl ether, and methanol, respectively. Carboxylic acids in the F3A fraction were methylated (Me) with acidic methanol at 60° C for 4–12h, yielding fatty acid methyl esters. Fatty acid methyl esters in the F3AMe fraction were isolated from molecules such as hydroxy acids containing additional functional groups using silica gel columns (as above), where the F2 fraction contained the fatty acids for analysis.

n-Alkane and fatty acids were quantified and characterized on an Agilent gas

chromatograph (Agilent 7890A GC) with DB-5 column (30 m length, 250 mm ID) and a mass selective detector (5975C MSD) and flame ionization detector (FID). One microliter of sample dissolved in 100 μl hexane was injected into a multi-mode inlet injector at 60° C (0.1 min hold), which was then ramped to 320° C at 900° C per minute and held for the duration of the analysis.

The initial GC oven temperature was set at 60° C and ramped to 150° C at 15° C per minute, then ramped to 320° C at 4° C per minute and held there for the duration of the analysis. The sample, carried by a He stream was quantitatively split to the MSD and FID detectors through a microfluidics device downstream of the column. Compound identification was done with comparison of mass spectra and retention times to authentic standards, and quantification was done by integrating peak areas of the mass 57 ion for *n*-alkanes and the mass 74 ion for fatty acids. *n*-Alkyl lipid concentrations were calculated based upon the peak area of known concentrations of internal standards added to the TLE. We used a response factor correction to account for ionization biases between the 5α-androstane standard (a synthetic steroid) and the *n*alkanes for more accurate quantification of concentrations.

Carbon isotope ratios of *n*alkanes and fatty acids were analyzed using a Thermo Trace GC coupled to a Thermo Delta V isotope ratio mass spectrometer through an Isolink combustion interface at the Lamont Doherty Earth Observatory (LDEO) Stable Isotope Laboratory. All sample injections were interspersed with injections of molecular mixtures with known isotopic values (mixes A4, A5 and F8 supplied by Arndt Schimmelmann, Univ. of Indiana) that were used for correction of carbon isotope values. Fatty acid $\delta^{13}C$ values were corrected for the addition of the methyl group using a mass balance equation and the measured $\delta^{13}C$ value of the methanol used for methylation. All $\delta^{13}C$ values were corrected for analytical uncertainty, including the ref

gas uncertainty, using a Matlab script as described in Polissar and D'Andrea (2014).

2.2.5. Enamel sampling, pretreatment, and isotope analysis

Sampling of fossil teeth for stable isotopes was performed by KU in Abu Dhabi and at the University of Utah. Fossil teeth were selected from nine mammalian families. Prior to drilling, each tooth was inspected, photographed, and a sampling location on the tooth was evaluated.

The sample protocol for bulk sampling involved sampling along broken enamel surfaces whenever possible, or in some cases a lateral tooth surface, using a Dremel handheld drill with carbide (Brasseler) or diamond grit impregnated (Lasco) bits at low speed (~2000 RPM). No occlusal surfaces were drilled. The sample surface was prepared by abrading the enamel surface with the drill bit. On lateral surfaces, this removed surface adherents and the outermost enamel (*ca.* 100 μm). If present, cementum was drilled away to expose enamel. After visual inspection of the prepared surface with a hand lens, a narrow groove about 1mm deep and 1 to 2 mm wide was drilled parallel to the growth axis of the tooth. Sample groove lengths varied based on tooth geometry imposed additional constraints (enamel thickness and crown length), but ideally were 10 to 15 mm long to average out potential seasonal variability in diet and water. Sample masses ranged from about 3 to 15 mg.

Six equid molars were serially sampled along the growth axis of the tooth to generate intratooth isotope profiles. Cementum was cleared away using the Dremel to expose a window of the fossil enamel. The exposed area was ~5mm wide and ran the length of the tooth crown (30 to 60 mm). Samples were drilled every 3 mm along the growth axis of the tooth, with sample grooves oriented normal to the growth axis. Sample grooves were ≤ 1 mm deep, ~1 mm wide,

and 3 to 6 mm long. Sample masses were about 2-5 mg.

Enamel powders from bulk and intratooth profile samples were pretreated prior to stable isotope analysis with 3 % NaOCl (bleach) for 30 minutes in 1.7 ml centrifuge tubes that were stirred every 10 minutes on a vortex mixer. After the reaction period, samples were centrifuged and the supernatant was removed. Each sample was then rinsed three times with distilled water. The rinse procedure involved adding de-ionized (DI) water, stirring on the vortex mixer, then centrifuging the sample and removing the supernatant. Next, samples were treated with 0.1 M Na-acetate buffered acetic acid for 30 minutes, as above, and following three distilled water rinses were loosely covered and dried overnight in a fume hood. Approximately 300 to 600 μg of powdered enamel sample was weighed out into silver capsules, along with NBS-19 standard (20-50 μg) and internal enamel standards. Samples and standards were roasted *in vacuo* for 2 hours at 60° C to remove adsorbed water.

Serial samples were analyzed at the University of Utah using a Finnigan Carboflo device coupled to a MAT 252 isotope ratio mass spectrometer (IRMS). Enamel samples were reacted with phosphoric acid at 90° C for 10 minutes under a He stream and exsolved CO_2, produced from the H_3PO_4 reaction, was cryogenically focused in a liquid nitrogen trap. The CO_2 was cryogenically transferred to a microvolume at −170° C and then inlet into the IRMS via dual inlet mode at −60° C.

Bulk enamel samples were analyzed at the LDEO Stable Isotope Laboratory using a Kiel IV device coupled to an IRMS. The Kiel differs from the CarboFlo in that it uses single reaction vessels rather than a common acid bath. As such, bulk enamel samples were transferred from silver capsules to round bottom, glass reaction vials after roasting *in vacuo*. A strand of silver

wool was added to each vial to oxidize any SO_2 produced in the reaction. Sample vials were loaded into the Kiel, where they were reacted with phosphoric acid at 70° C for 10 minutes in vacuo. Exsolved gases were cryogenically transferred to a microvolume held at −170° C, and then transferred to second microvolume with the first held at −70 °C to remove water. The purified sample CO2 was inlet to a dual-inlet Delta V Plus IRMS.

All carbon and oxygen isotope ratios were corrected using international and internal standards. The standard deviation of NBS-19 throughout sample runs was ~0.05 ‰ for $\delta^{13}C$ and <0.10 ‰ for $\delta^{18}O$. Oxygen isotope values were converted from CO_2 (gas) to fossil enamel (mineral) values using temperature dependent fractionation factors (1.00799 for 70° C; 1.00725 for 90° C) using the equation for fossil enamel (Eq. 4) in Passey et al. (2007).

We combine bulk tooth enamel carbon and oxygen isotope data analyzed for this study (n = 35) with those previously published (n = 30) by Kingston (1999). In order to compare the $\delta^{18}O$ values from Kingston (1999) to those determined in this study, we recalculated values from the previous study, originally calculated using the calcite-based acid fractionation factor, using a tooth enamel specific, temperature dependent acid fractionation factor (Eq. 3) from Passey et al. (2007). This is necessary so that the $\delta^{18}O$ values from both data sets can be directly compared. To do this, we converted the $\delta^{18}O$ values from mineral back to CO_2 (gas) $\delta^{18}O$ values using the commonly applied calcium carbonate acid fractionation factor of 1.01025 (Swart et al., 1991). We then apply the tooth enamel acid fractionation factor from Passey et al. (2007) for a sealed vessel reaction at 70° C, where α = 1.00799, so that the Kingston (1999) data are placed in the same reference framework as our data. The difference between the originally published and

recalculated $\delta^{18}O$ values for the modern enamel samples is on the order of +2.4 ‰.

2.2.5.1. Intratooth stable isotope profiles and inverse modeling

Intratooth isotope profiles of herbivore tooth enamel provide a time series of the diet and body water over the period in which the tooth enamel formed (Fricke and O'Neil, 1996; Sharp et al., 1998). For obligate drinkers such as equids, the $\delta^{18}O_{enamel}$ values track meteoric water (Huertas et al., 1995). This is supported by feeding and drinking observations, which show that in warm environments with air temperatures similar to Abu Dhabi today (30 to 35 °C), mares drink every ~2 hrs during the heat of the day(Crowell-Davis et al., 1985). Thus, the first order control on $\delta^{18}O_{enamel}$ is meteoric water. In extant equids, premolars and molars form over 1.5 to 2.8 years, inclusive of crown extension and enamel maturation (Hoppe et al., 2004). The time represented in intratooth isotope profiles can therefore be used to evaluate seasonal variability in precipitation, vegetation, and diet (Metcalfe et al., 2011; Nelson, 2005; Sharp et al., 1998).

Amelogenesis, or the process of enamel formation, is a two-stage process that starts with a secretory stage, when enamel matrix is deposited, followed by a protracted maturation stage, when density of the original matrix increases significantly (Suga, 1979). As a result, the isotope ratio of a given volume of enamel represents a time integrated signal of the initial period of matrix deposition and the period of maturation. Tooth enamel maturation and isotope sampling methods blur and attenuate the original isotope input signal (Passey & Cerling, 2002; Zazzo et al, 2005). To unblur the signal, we apply the inverse method developed by Passey et al. (2005) to estimate the original input signals for $\delta^{13}C_{enamel}$ (diet) and $\delta^{18}O_{enamel}$ (body water) that more closely reflect the actual diet and body water composition of the equid during the time during in

which the tooth formed. The inverse model requires input parameters that related to tooth formation, isotope sampling geometry, and isotope analysis. Input parameters relevant to tooth enamel formation, or amelogenesis, include initial enamel density (f_i), enamel appositional length (l_a) and maturation length (l_m) (Passey and Cerling, 2002). We use parameters measured on *Equus ferus przewalskii* by (Blumenthal et al., 2014) as estimates for equid molars used here, where f_i = 22 %, l_a = 6 mm, l_m = 28 mm. Sample input variables include distance between samples (3 ± 0.5 mm) and depth (0.7 mm ± 0.2 mm). The final input variables are the measured carbon and oxygen isotope data and their associated uncertainties, which were smoothed with a 3-point weighted mean (0.25:0.5:0.25). A measured error term, E_{meas}, is computed from measurement uncertainties in isotope values and sample measurements. This term ultimately governs model sensitivity that is then used to determine an appropriate damping factor (ε). The model requires selection of a damping factor that minimizes the difference between E_{meas} and the prediction error (E_{pred}). A detailed description of additional model parameters and the regularization method is given in Passey et al. (2005). Model code was downloaded and adapted from Passey et al. (2005). While it is widely accepted that ungulate cheek teeth have non-linear growth rates, particularly towards the base of the of crown (Bendrey et al., 2015; Zazzo et al., 2012), the inverse model requires us to assume a constant growth rate. The difference between linear vs. exponential growth rates has the greatest effect in the lowermost portion of the crown. Across the main part of the crown, a linear approximation of growth rate is reasonable (see fig. 4 in Bendrey et al., 2015). We sampled teeth in this study that were not heavily worn so most samples come from regions of the teeth where growth rates can be approximated as linear.

Further work on the mode and rates of growth in ungulate cheek teeth may help produce even more precise models in the future.

2.2.6. Climate and precipitation records

Meteorological and soil data collected from 1971-1999 at the Abu Dhabi weather station (WMO Station #41216 at the Bateen Airport; 24.43° N, 54.45° E) are used to establish a modern baseline for monthly precipitation, mean annual precipitation (MAP), monthly temperature, mean annual temperature (MAT), and maximum monthly mean soil temperature from the NOAA database (NOAA, 2018) (Fig. 18.2). The average $\delta^{18}O$ value of precipitation for Abu Dhabi is calculated using the average of three values from the area. The first estimated value is from published $\delta^{18}O$ data for the closest GNIP station (WMO Station # 4115001 at the Bahrain Airport, 26.27° N, 50.62°E) located ~320 km northwest of the Baynunah fossil sites (IAEA/ WMO, 2019). The second is from a published $\delta^{18}O$ value for United Arab Emirates (UAE) precipitation (Rizk and Alhsharhan, 2003). The third is an estimate for the fossil site region using the Online Isotope Precipitation Calculator (2015; Bowen, 2018; Bowen and Revenaugh, 2003).

Fig. 18.2 near here. Width = 1 column

Modern climate data are compared to water isotope data reconstructed from oxygen isotopes in pedogenic carbonate (Kingston, 1999) and tooth enamel (Kingston, 1999; this study). Mineral phase (carbonate and apatite) oxygen isotope ratios (PDB) are converted to water

oxygen isotope ratios (VSMOW) using the equation for determining the isotope fractionation by Kim and O'Neil (1997).

In the case of pedogenic carbonates, we calculate soil water oxygen isotope values ($\delta^{18}O_{sw}$) using the reported maximum monthly mean modern soil temperature of 35° C at 50 cm depth in Abu Dhabi as an estimate for late Miocene soil temperatures (NOAA, 2018). For tooth enamel, we calculate body water oxygen isotope values ($\delta^{18}O_{bw}$) of Baynunah hippos. Due to their semi-aquatic habitat, hippo $\delta^{18}O_{bw}$ values best reflect meteoric water (Bocherens et al., 1996; Cerling et al., 2008; Levin et al., 2006). We apply the same Kim and O'Neil (1997) equation using a standard mammalian body temperature of 37° C. This yields an enrichment factor ($\varepsilon_{bw\text{-}en}$) between body water $\delta^{18}O$ ($\delta^{18}O_{bw}$) and enamel $\delta^{18}O$ ($\delta^{18}O_{en}$) of 26.0 ‰, which is nearly identical to the experimentally derived value of 26.3 ± 0.14 ‰ determined by Bryant et al. (1996). Taken together, reconstructed soil water and hippo body water $\delta^{18}O$ values can be compared to the modern measured (GNIP database and Rizk and Alhsharhan, 2003) and OIPC modelled $\delta^{18}O$ of precipitation values.

3. Results

3.1. Plant waxes

3.1.1. Plant wax concentrations

Plant wax concentration, CPI, and ACL for seven samples from four sites – HMR 5, KIH 2, MLS 1, and RUW SE – are given in Table 18.2. Plant wax concentrations range from 1.8 to 64.6 ng/g sediment for the *n*-C_{31} alkane and 0.4 to 66.0 ng/g sediment for the *n*-C_{30} fatty acid, both of

which are generally the most commonly reported homologs for their compound classes. For the *n*-alkanes, most samples exhibit a C_{31} maximum with high abundances of C_{29} and C_{27} homologs and low abundances of the longer chain homologs, C_{33} and C_{35}. Fatty acid samples have compound maxima ranging mostly from C_{24} to C_{28}. Relative abundances of *n*-alkane and fatty acid chain-lengths are illustrated in Fig 18.3. *n*-Alkane CPIs range from 3.1 to 6.7 and fatty acid CPIs range from 2.2 to 2.6. These CPI values all indicate preservation of the primary plant wax signal. *n*-Alkane ACLs range from 28.8 to 30.5 and whereas fatty acid ACLs are slightly shorter, ranging from 27.0 to 28.0.

Fig. 18.3 here. Width = Full page width

Table 18.2 near here. Width = full page

Overall, the concentrations, CPI, and ACL all indicate preservation of the primary plant wax signal for the longer chains ($\geq C_{30}$), and we note some samples have lower CPIs across the midchain regions, potentially from algal, aquatic macrophytes, or post depositional processes. This is evident in fatty acid samples from KIH 2, MLS 1, and some from HMR 5. These midchain homologs are also present, although to a lesser degree, in the *n*-alkane samples (Fig. 18.3). They do not have a significant effect on the longer chain carbon isotope ratios or the vegetation reconstructions.

3.1.2. Plant wax stable isotope ratios

Carbon isotope ratios range from −29.2 to −22.0 ‰ for long chain *n*-alkanes (C_{27} to C_{35}, Fig. 18.4). The C_{31} alkane ranges from −29.2 to −22.6 ‰, which results in an estimated 27 to 73 % C_4 (median = 43 %C_4) vegetation on the landscape (Table 18.3). The C_{35} alkane, a sensitive indicator of C_4 vegetation, ranges from −26.4 to −23.1 ‰. Fatty acids $\delta^{13}C$ values from all homologs range from −30.6 to −21.5 ‰, similar but slightly larger than the range observed in the *n*-alkanes (Fig. 18.4). The C_{30} fatty acid ranges from −28.9 to −22.9 ‰, nearly identical to the range observed in the C_{31} alkane. The biomarker sample from site MLS 1, a locality known for its preservation of a remarkable proboscidean trackway (Bibi et al., 2012), was the most open landscape with an estimated 73 %C_4 vegetation. Samples from HMR and KIH 2 yield similar $\delta^{13}C_{alkane}$ values and indicate mixed ecosystems ranging from 36 to 52 %C_4 vegetation. The sample from RUW SE had the lowest amount of C_4 vegetation (27 %).

Fig. 18.4 near here. Width = full page.

Table 18.3 near here. Width = full page

3.2. Stable Isotopes in Teeth

3.2.1. Pretreatment results

Eleven samples were analyzed with and without pretreatment (Figure 18.5). There is no difference in mean carbon values between treated and untreated samples (0.0 ‰), low variability (1σ = 0.3 ‰), and a small absolute difference of 0.6 ‰ (Table 18.4). For oxygen, the mean difference is similarly small (0.1 ‰), but variability (1σ = 1.2 ‰) and the absolute difference,

2.3 ‰, is high (Table 18.4). The slope of treated vs. untreated for both isotopes is close to 1 (Fig. 18.5).

Fig. 18.5 near here. Width = full page

Table 18.4 near here. Width = full page

3.2.2. Bulk samples

Carbon and oxygen isotope values from fossil enamel yielded a wide range of values. Here we include analyses of fossil tooth enamel from Kingston (1999) for a total of 65 fossil teeth analyzed from Baynunah (Figure 18.6; Table 18.5). We include in Table 18.5 the original $\delta^{18}O$ values provided in Kingston (1999, Table 1), but plot them all in the same reference framework as described in section 2.2.5. For carbon, the $\delta^{13}C_{enamel}$ values ranged from −13.2 ‰ to +0.9 ‰, with a median value of −2.2 ‰. Oxygen isotope values ranged −8.9 ‰ to +8.5 ‰, with a median value of −2.9 ‰ (Table 18.5). Plotting tooth enamel stable isotope data by family illustrates the wide range of carbon and oxygen values at Baynunah (Fig. 18.7). The carbon isotope ratios were converted to percent C_4 in diet using equation (2), resulting in diets ranging from 0 to 84 % C_4, with a median value of 63 %C_4. Propagated uncertainty in %C_4 is reported in Table 18.5 and ranges from 12 to 23 % (median 12%), which should be noted in the ensuing discussions of diet. Only 15% of the sampled individuals had C_3-dominated diets, about two-thirds (65%) had mixed C_3-C_4 diets, and the remaining 20 % had C_4-dominated diets. Most individuals (62%) had diets consisting of ≥50 %C_4, confirming that C_4 was the primary dietary source for Baynunah herbivores.

Fig. 18.6 near here. Width = 1 column

Fig. 18.7 near here. Width = full page

Table. 18.5 near here.

3.2.2.1. Artiodactyls

Box plots for carbon and oxygen are shown for bovids, giraffids, hippopotamids, and suids in Fig. 18.7. Bovid $\delta^{13}C_{enamel}$ ranges from −10.4 to +0.1 ‰, and $\delta^{18}O_{enamel}$ from −3.7 to +0.4 ‰ (n=5). The corresponding amount of C_4 vegetation in diet is 7 to 79 % (median 36%, Table 18.5). Taxa include two *Pachyportax latidens* (51 and 79 %C_4), two *Tragoportax cyrenaicus* (7 and 36 %C_4), and one indeterminate bovid. Giraffid isotope values have an impressively wide range, with $\delta^{13}C_{enamel}$ values ranging from −9.2 to +0.2 ‰, with corresponding diets of 15 to 79 %C_4 (median = 64 %; n=6). Girrafid $\delta^{18}O_{enamel}$ values range from −2.6 to +8.5 ‰, and include the highest values recorded from Baynunah. Hippopotamids, represented by *Archaeopotamus qeshta*, yield $\delta^{13}C_{enamel}$ values ranging from −5.5 to +0.3 ‰ and $\delta^{18}O_{enamel}$ values ranging from −8.2 to −3.3 ‰ (n=11). Hippopotamid diets range from 40 to 80 %C_4 (median = 73 %). Two *Nyanzachoerus syrticus* and one *Propotamochoerus hysudricus* specimens give a narrow range of $\delta^{13}C_{enamel}$ values. Suids are mainly at the C_3 end of the range, from −11.1 to −9.7 ‰, which translates to 2 to 11 %C_4 (n=3). Suid $\delta^{18}O_{enamel}$ values range from −3.7 to −0.4 ‰. It is not known if the two suids from the Baynunah Formation were herbivores or omnivores, but presumably even omnivorous suids would have diets dominated by plant matter, and their enamel carbon isotope values must therefore reflect the vegetational composition of the diet.

3.2.2.2. Perissodactyls

Perissodactyls are represented by Equidae and Rhinocerotidae. The former are very common and the latter extremely rare in the Baynunah Formation. Equids are assigned to "*Hipparion*" *abudhabiense* and a smaller sized *"Hipparion"* (Bernor et al., Chapter 16, this volume). Equid values range from −7.8 to +0.9 ‰ for $\delta^{13}C_{enamel}$ and from −5.9 to +1.8 ‰ for $\delta^{18}O_{enamel}$ (n=24); (Fig 18.7). Diets of equids range from 24 to 84 %C_4 (median = 63 %). The two rhinocerotid specimens were enamel fragments attributable only to the family level and have nearly identical $\delta^{13}C_{enamel}$ values (−10.4 and −10.2 ‰) and $\delta^{18}O_{enamel}$ values (−3.9 and −3.7 ‰), with corresponding diets of 7 to 9 %C_4.

3.2.2.3. Proboscideans

Fossils representing three proboscideans lineages, the Elephantidae, Deinotheriidae, and Gomphotheriidae, have been recovered from the Baynunah Formation (Sanders, Ch. 10, this volume). The most common by far is the newly erected elephantid species, *Stegatetrabelodon emiratus*, which has $\delta^{13}C_{enamel}$ values of −7.3 to −0.2 ‰ and $\delta^{18}O_{enamel}$ values of −4.2 to +2.2 ‰ (Fig 18.7). *Stegatetrabelodon emiratus* diets range from 28 to 77 %C_4 (median = 65 %). The two deinotheriid (aff. *Deinotherium bozasi*) teeth sampled yield the most negative values from the Baynunah Formation measured to date, −13.2 and −12.4 ‰, corresponding to pure C_3 diets. The $\delta^{18}O_{enamel}$ values are −3.0 and −0.2 ‰. A single and somewhat enigmatic gomphotheriid tooth originally assigned to *Stegotetrabelodon grandincisivus* and now more conservatively assigned to Gomphotheriidae gen et sp. indet by Sanders (this volume), has a $\delta^{13}C_{enamel}$ value of

−4.3 ‰ (48 %C_4) and a $\delta^{18}O_{enamel}$ value of −1.1 ‰, which both fall within the range of values observed for *S. emiratus* (Fig. 18.7).

3.2.3. Serially sampled equids

The measured $\delta^{13}C_{enamel}$ and $\delta^{18}O_{enamel}$ values of six serially sampled equid teeth range from −7.1 to +0.7 ‰ and from −6.8 to +1.1 ‰, respectively (n=84, Table 18.6). The modeled ranges for both are larger, as expected because the model 'unblurs' the tooth enamel signal by accounting for sampling geometry and amelogenesis (Fig 18.8). Modeled $\delta^{13}C_{enamel}$ and $\delta^{18}O_{enamel}$ ranges from all profile samples are −8.2 to +2.7 ‰ and −7.1 to +4.4 ‰, respectively. For the modeled carbon data, this is equivalent to diets ranging from 22 to 97 %C_4 vegetation (median = 56%). Within a single profile, the maximum modeled $\delta^{13}C_{enamel}$ range is from −8.2 to −1.9 ‰ (AUH 1566), equivalent to a 22 to 65 %C_4 range in diet. The average modeled $\delta^{13}C_{enamel}$ range is 5.3 ± 0.8 ‰ (1σ) (Fig 18.8). The highest range in the modeled $\delta^{18}O_{enamel}$ data is from −6.2 to +4.4 ‰ (AUH 1295) and the average range within a profile is 8.1 ± 2.2 ‰.

Fig. 18.8 near here. Width = fit to page

Table. 18.6 near here.

Overall, the intratooth profiles exhibit quasi-periodic patterns of variability in both carbon and oxygen isotopes (Fig 18.8). The general trend is that $\delta^{13}C_{enamel}$ values covary inversely with $\delta^{18}O_{enamel}$ values, whereby more positive $\delta^{13}C_{enamel}$ values occur with more

negative $\delta^{18}O_{enamel}$ values. Assuming the quasi-periodic cycles in the intratooth isotope profiles represent annual seasonality of vegetation and hydroclimate, then overall growth vertical rates of the equid cheek teeth can be estimated as 2.5 to 4 cm/yr , similar to the estimated growth rate in modern horses of 3 to 4 cm/year (Hoppe et al., 2004).

3.2.4. Baynunah Hydroclimate

Meteorological and soil data from the Abu Dhabi weather station (WMO Station #41216; 24° 26'N, 54° 28'E) record a mean annual precipitation (MAP) of 57 mm and a mean annual temperature (MAT) of 27° C. Reported modern soil temperature of 35°C is in excess of mean annual air temperatures, which is commonly observed in arid ecosystems (Passey et al., 2010; Quade et al., 2013). The estimated $\delta^{18}O$ values for annual precipitation ($\delta^{18}O_{precip}$) are given in Table 18.7 and have a mean value of +0.5 ‰ (VSMOW), which is reasonable for a hyperarid region with very low rainfall.

Table. 18.7 near here.

In contrast, we calculate a late Miocene mean $\delta^{18}O$ soil water ($\delta^{18}O_{sw}$) value of −3.9 ± 1.2 ‰ (VSMOW) from pedogenic carbonate data (Kingston, 1999), and hippo $\delta^{18}O_{bw}$ values ranging from −3.5 to +0.8 ‰ (median −1.2 ‰, VSMOW). Taken together, reconstructed soil water and hippo body water values indicate that late Miocene precipitation was more negative than modern values by ~4 ‰. As a caveat however, in some cases, such as in arid environments or closed

lakes, the $\delta^{18}O$ of water and thus of hippo body water does not necessarily reflect precipitation because of evaporative enrichment.

4. Discussion

4.1. Paleoenvironmental reconstructions in Local and Regional Contexts

4.1.1. Baynunah vegetation from carbon isotopes

The plant wax carbon isotope data from *n*-alkanes and fatty acids show good agreement between the two classes of plant waxes and indicate mostly mixed C_3-C_4 ecosystems, which likely comprised grassy woodland or bushland to wooded or bushy grasslands (Fig. 18.4). The plant wax carbon isotope data agree well with that from pedogenic carbonate and also from diet-based reconstructions from enamel. All point to mixed C_3-C_4 ecosystems. Carbon isotope data from plant waxes and pedogenic carbonate indicate ranges of 27 to 73 % C_4 and 16 to 63 % C_4, respectively (Table 18.8). Two-thirds of the sampled large herbivore teeth indicate mixed C_3-C_4 to C_4-dominated diets (Fig. 18.7), further supporting the plant wax and pedogenic carbonate data.

Table. 18.8 near here.

We evaluate the vegetation signals from sites where multiple carbon isotope proxy data are available (Hamra, Kihal, Jebel Barakah, Shuwaihat, and Ruwais) to explore the range of possible environments in the Baynunah (Table 18.8). Temporal and stratigraphic correlation between Baynunah sites is problematic owing to the difficulties of precisely dating the sediments

and to the heterogeneous nature of fluvial sediments in a variable, broad depositional system (Friend, 1999; Schuster, Ch. 3, this volume). The sites are all broadly contemporaneous, however, and differences in reconstructed vegetation therefore likely reflect spatial landscape heterogeneity over the timescale of deposition, which may have been on the order of one to several hundred thousand years (Peppe, Ch 18.4, this volume; Hailwood and Whybrow, 1999).

Sites at Kihal (KIH 2) and Hamra (HMR 5) both yielded multiple plant wax and pedogenic carbonate samples that indicate mixed vegetation (16 to 62 %C4, Table 18.8). Tooth enamel data from Hamra (HMR 1, 2, 3 ,5 ,6) and Kihal (KIH 1 and UL) similarly indicate a wide range of diets (2 to 79 $\%C_4$ and 62 to 82$\%C_4$, respectively). The median dietary values from these sites (65 $\%C_4$ and 72 $\%C_4$), are in good agreement with the higher end of $\%C_4$ estimates from the plant wax and pedogenic carbonate data at those sites. At the westernmost site, Jebel Barakah, pedogenic carbonate data (JBR 2, 3, and '20') indicate 32 to 55 $\%C_4$ vegetation whereas enamel data (JBR 'east', 2, '20', and UL) suggest 40 to 84 $\%C_4$ vegetation in diets. A single pedogenic carbonate sample from Shuwaihat (SHU 8) shows 63 $\%C_4$ vegetation, where a large sample of enamel indicates diets ranged from 0 to 78 $\%C_4$ (SHU 1, 2, and 4). A single plant wax sample from Ruwais (RUW SE) yielded the most negative $\delta^{13}C_{alkane}$ value, representing an estimated 27 $\%C_4$ vegetation. In contrast, a single hippo from this site had a mixed but mostly C_4 diet (67%). Finally, at Mleisa (MLS1), the site of a proboscidean herd trackway (Bibi et al., 2012), a single plant wax sample indicates 73 $\%C_4$, the highest recorded value in the Baynunah. The most abundant proboscidean and most likely to be found in the open environment at Mleisa is *S. emiratus* (Bibi et al., 2012; Sanders, Ch. 10 this volume), which has a median diet of 65 $\%C_4$. Mazzini and Kovacova (Ch. 6, this volume) reconstruct the Mleisa (MLS1) trackway site

as a low energy, non-marine, seasonally-inundated plain based on ostracod and charophyte fossil remains. Such a brackish, fluctuating wet-dry environment may have supported C_4 sedges, grasses, or halophytic C_4 shrubs (e.g., Amaranthaceae or Chenopodaceae). Sedimentological evidence also points to periodic drying of the carbonate-rich sediment based on desiccation cracks (Bibi et al., 2012).

4.1.2. Old World vegetation from carbon isotopes

The vegetation reconstruction from carbon isotopes in pedogenic carbonates enables a direct comparison of Baynunah ecosystems with those of contemporaneous sites in South Asia, the Siwaliks, and in eastern Africa, Lothagam (Fig. 18.9). The timing and rate of the spread of C_4 vegetation differ between the African and South Asia. The onset of the C_4 expansion in Africa started at ~10 Ma, whereas C_4 vegetation spread more rapidly in South Asia than in Africa, starting at ~7.5 Ma (Behrensmeyer et al., 2007; Feakins et al., 2013; Polissar et al., 2019; Quade et al., 1989; Uno et al., 2016a). The age uncertainty of the Baynunah Formation precludes comparisons about the timing and rate of diet and ecosystem change between the other sites, but the carbon isotope data still provide a basis for which to compare vegetation in the context of woody cover. Data compiled from all sites ranging from 8 to 6 Ma (Behrensmeyer et al., 2007; Cerling et al., 2003a; Kingston, 1999), updated to the GPTS of Gradstein and Ogg (2012) where relevant and converted to fraction woody cover using the equation of Cerling et al. (2011), (Fig. 18.10). As a functional classification, Cerling et al. (2011) use >80 % woody cover to denote forest habitats, 80 to 40 % as (grassy) woodland, bushland, or shrubland, 40 to 10% as woody grasslands, and <10 % as grasslands. The data indicate that Baynunah and Lothagam were

similar to each other, with 74 and 76 % of the values, respectively, indicating woody grasslands, and ca. 5 % of the values indicating grasslands (Table 18.9). Only *ca.* 25% of values at these sites have *fwc* > 40 %. In contrast, during the same late Miocene interval in the Siwaliks, more than 72 % of the data indicate woody-dominated ecosystems (fwc > 40 %), with woody grasslands and grasslands making up 24 and 4 % of the Siwaliks data set, respectively (Figure 18.10).

Fig. 18.9 near here. Width = full page.

Fig. 18.10 near here. Width = half page.

Table 18.9 near here

4.1.3. Hydroclimate Evidence for Monsoon Conditions

The climate of the Baynunah region today is characterized by warm temperatures and very low mean annual precipitation that results in a hyperarid ecosystem incapable of supporting the diversity of large mammals that lived there during the late Miocene. Conditions during the late Miocene were clearly much wetter than present and the ensuing discussion aims to provide isotopic evidence for a wetter and highly seasonal climate.

The late Miocene $\delta^{18}O_{sw}$ value, which is a maximum estimate of the $\delta^{18}O_{precip}$ due to soil water evaporation, is 4 ‰ more negative than the estimated modern-day $\delta^{18}O_{precip}$ (Table 18.7). There are three major mechanisms that could lead to such a difference between late Miocene and modern $\delta^{18}O$ values. The first is the amount effect, whereby higher precipitation amounts result

in lower $\delta^{18}O_{precip}$ values (Dansgaard, 1964). The second is what is often called the continental effect, whereby an increase in the distance between the site of precipitation and the source water results in a decrease in the $\delta^{18}O_{precip}$ value through Rayleigh distillation (Dansgaard, 1964). The third mechanism is changes in the temperature of source water (i.e., sea surface temperature), which affects the fractionation factor between liquid and vapor during evaporation.

The amount effect, or higher MAP, is the most likely cause for the more negative $\delta^{18}O$ values in the late Miocene. The amount effect is the dominant control on isotopic variability in precipitation in low latitudes, where mean annual temperature variability is small and therefore the temperature effect on the $\delta^{18}O_{precip}$ is low. Multiple lines of evidence supporting our interpretation of the oxygen isotope values as indicative of higher MAP include geological, paleontological, modeling, and geochemical data. The fluvial deposits of the Baynunah Formation provide evidence for a variable but primarily low energy, braided river system, which requires regionally wetter conditions than present (Friend, 1999; Schuster, Ch. 3 this volume). Other sedimentary facies, such as ostracod rich carbonate muds at Mleisa, provide evidence for local, seasonally inundated fresh to brackish environments (Bibi et al., 2012; Mazzini and Kováčová, Ch 6 this volume.). The assemblage of large mammals and the associated ecosystems required to support their diet and water needs also point to higher rainfall in the region.

Vegetation reconstructions also provide clues about the rainfall regime of the Baynunah sites. Modern savannas are a good analogue for the mixed C_3-C_4 ecosystems that existed at Baynunah. In modern African savannas—the savanna ecosystems that are closest geographically and floristically to the Arabian Peninsula—MAP ranges from ~150 to 1200 mm (Sankaran et al., 2005), which provides a general constraint for the late Miocene Baynunah. A late Miocene

climate model covering much of Asia and the Arabian Peninsula suggests that annual and seasonal temperature and precipitation values in the late Miocene were not greatly different than those today, with perhaps slightly wetter summers and slightly drier winters (Tang et al., 2011). A Pleistocene reconstruction of Arabian paleoprecipitation from an ensemble of GCM models suggests a MAP of 200 to 600 mm for the Baynunah region during the last interglacial, ~130 ka (Jennings et al., 2015). The best precipitation estimate for the Baynunah during the late Miocene comes from modeling by Zhang et al. (2014). Their data show the Baynunah region crossed by the 800 mm MAP isopleth (and bounded between 400 to 1200 mm MAP isopleths), where the higher MAP compared to the modern is largely due to the more northerly position of the Intertropical Convergence Zone in the late Miocene. Around 800 mm MAP falls within the range of rainfall for modern savanna ecosystems and therefore seems a reasonable estimate for the late Miocene Baynunah.

Whereas multiple lines of evidence suggest higher precipitation in the late Miocene, there is less support for the other two possible mechanisms contributing the observed decrease in $\delta^{18}O$ values. Changes in the vapor source or transport distance were likely minimal because there have not been changes in regional paleogeography since the late Miocene that would significantly affect the distance of the Baynunah region to the Arabian Sea and Indian Ocean, which were the likely moisture sources for precipitation (Fig. 18.9 and see figure 9 in (Popov et al., 2004). Therefore, we rule out the influence of vapor transport distance on the changes in $\delta^{18}O$ values. The third possible mechanism, a change in source water temperature, is not likely responsible for the observed $\delta^{18}O$ values. This would require cooler SSTs when in fact Arabian

Sea SSTs were about 2 to 3° C warmer in the late Miocene compared to present (Huang et al., 2007; Zhuang et al., 2017).

The intratooth oxygen isotope profiles and the inverse model results from equid teeth provide new and important information that support a highly seasonal, monsoonal precipitation regime. We interpret the intratooth profile data from the Baynunah equids as indicating a single rainy season represented by more negative $\delta^{18}O_{enamel}$ values, followed by a long dry season with more positive $\delta^{18}O_{enamel}$ values (Fig. 18.8). This interpretation fits the relationship observed where the amount effect is dominant. In a study of modern equids, Blumenthal et al. (2019) show that the $\delta^{18}O_{enamel}$ range in intratooth profiles scales with the $\delta^{18}O$ range in precipitation in low latitudes. The lower $\delta^{18}O$ precipitation values in the tropics generally corresponds to wet seasons. The modern equid data support for the interpretation of the Baynunah data.

The corresponding equid $\delta^{13}C_{enamel}$ profiles in turn reveal increased C_4 feeding during the wet season – presumably the preferred diet – and increased C_3 feeding during the dry season – presumably the fall-back resource (Fig. 18.8). The modeled intratooth $\delta^{18}O_{enamel}$ ranges are very high, approaching 11 ‰, indicating strong seasonality. These isotopic data can not be simply converted to absolute rainfall values, but the *measured* range of $\delta^{18}O_{enamel}$ values in Baynunah equids (4.7 ± 0.9 ‰) is more than 2 ‰ greater than the range observed in coeval (8 to 6 Ma) profiles from equid teeth from the Siwaliks (2.6 ± 0.8 ‰; (Nelson, 2005). This suggests much greater seasonality of precipitation in the Baynunah than in the Potwar Plateau of Pakistan during the late Miocene. While seasonal variability in the $\delta^{18}O$ values of meteoric water likely

dominate the $\delta^{18}O_{enamel}$ profiles, other factors such as changes in water source related to diet change or animal physiology and behavior likely play a secondary role.

Oxygen isotope data from bulk tooth enamel provide further evidence for strong seasonality (Fig. 18.7). There is a nearly 12 ‰ difference between the median values of the water-dependent hippos (low $\delta^{18}O_{enamel}$), and the less water-dependent giraffids (high $\delta^{18}O_{enamel}$). Following the terminology of Levin et al. (2006), hippos are an evaporation insensitive (EI) taxon whose $\delta^{18}O_{bw}$ values most closely track meteoric water, whereas giraffes are an evaporation sensitive (ES) taxon whose $\delta^{18}O_{bw}$ values are sensitive to aridity because a high fraction of their ingested water comes from leaf water that is subject to evaporative enrichment of ^{18}O by local aridity. The high $\delta^{18}O_{enamel}$ values of the giraffes stand out among other taxa in the Baynunah because it is the only ES lineage at the site (discussed below). Furthermore, the giraffe data stand out because most of the sampled teeth show mixed or C_4 diets that differ from extant giraffe diet and because they all come from the same site (RDB 2), so their anomalously high $\delta^{18}O_{enamel}$ values may reflect a highly localized signal. Thus, we refrain from applying the updated equation for calculating water deficit (WD, mm/yr) from Blumenthal et al. (2017) to the Baynunah enamel data. However, we note that the ~12 ‰ difference between ES and EI $\delta^{18}O_{enamel}$ is similar to that for the Lake Turkana (Kenya) region today, where WD is *ca.* 2300. The large $\delta^{18}O_{enamel}$ offset between ES and EI taxa demonstrate the Baynunah environment was characterized by high aridity, further supported by the large amplitude in the equid intratooth profiles.

We interpret the evidence for highly seasonal precipitation as indications of a well-developed monsoon. The presence of a single wet season is more like the situation seen today in the African Sahel or parts of the Indian Peninsula, rather than the dual rainy season of modern East Africa. The monsoonal climate would have exerted major controls on the local vegetation structure, with long dry seasons and concentrated precipitation resulting in a high abundance of C_4 grasses and low fraction of woody cover Good et al. (2011). Together, the intratooth carbon and oxygen isotope profiles provide evidence for the presence of intense, monsoon-style hydroclimate seasonality, with significant seasonal changes in vegetation.

Finally, the equid intratooth profiles from Baynunah and the Siwaliks indicate that in both regions a monsoon system exerted primary control of hydroclimate. The seasonality of precipitation was stronger at Baynunah based on the intratooth amplitude of $\delta^{18}O$. Intratooth profiles from coeval African Lothagam fauna could help constrain seasonality there during the late Miocene. Precipitation amounts at Baynunah are estimated at ~800 mm/yr based on regional climate models (Zhange et al., 2014), whereas at Lothagam, the ecometric approach suggests a MAP of 900 ± 500 mm (Fortelius et al., 2016).

4.2. Dietary Reconstructions in Local and Global Contexts

The Baynunah tooth enamel carbon isotope data indicate a wide range of diets among Proboscidea, Perissodactyla, and Artiodactyla, including species with C_3-dominated, mixed C_3-C_4, and C_4-dominated diets at Baynunah. The majority of species have mixed C_3-C_4 or C_4-dominated diets, which generally agrees with the grassy woodland (or bushland) to woody (or bushy) grassland ecosystems reconstructed from the plant wax and pedogenic carbonate isotopes.

Carbon isotope data show a range of 14 ‰ and the oxygen isotope data a range of almost 17 ‰ across Baynunah fauna. Under the vegetation and hydroclimate framework discussed above, we discuss dietary reconstructions for the Baynunah ungulates, using oxygen isotope data to further evaluate water use, reliance, and relevance to diet. These data are contextualized through comparison with published enamel isotope data of other late Miocene (8-6 Ma) faunas from the Siwaliks (Potwar Plateau, Pakistan), Lothagam (Turkana Basin, Kenya), and Toros Menalla, Chad, all of which have varying degrees of taxonomic affinities to the Baynunah fauna (Figs. 18.9 and 18.11). We focus our comparison of Baynunah enamel isotope data primarily to Lothagam and the Siwaliks, from where the largest data sets are available (Badgley et al., 2008; Uno et al., 2011). For the $\delta^{18}O$ data reported in Badgley et al. (2008), we were unable to verify whether or not some or all values were calculated using the temperature dependent acid fractionation factor determined for enamel as was done for the values presented from Baynunah (this study) and Lothagam (Uno et al., 2011). Furthermore, we also caution that due to limited sample size of enamel powders, Lothagam enamel samples were not pretreated the way that samples from Baynunah and presumably Badgley et al. (2008) were. Thus, there may be $\delta^{18}O$ offsets of ~± 2 ‰ relative to treated samples.

4.2.1.1. Artiodactyls

While at least eight species of Bovidae are present in the Baynunah fauna (Bibi, Ch. 14, this volume) only two species were sampled, the C_3-dominated to mixed feeding *Tragoportax cyrenaicus* and the mixed to C_4-dominated feeding *Pachyportax latidens*. Together, these two large species span a wide range of the C_3-C_4 dietary spectrum. These two species had diets more similar to bovids from Lothagam (Fig. 18.11) than from the Siwaliks, despite closer taxonomic

affinities with the latter. In the Siwaliks, bovids from 8 to 6 Ma still had mostly C_3-dominated to mixed diets, with only a few having C_4-dominated diets and almost none having the mixed diets. observed at Baynunah (Fig. 18.11). *Tragoportax pilgrimi* from the Siwaliks had a C_3-dominated diet from ~8.5 to 8 Ma but from 7.3 Ma onwards shows a mixed to C_4-dominated diet. Limited data from three *Pachyportax* samples from the Siwaliks, all from ~7.3 Ma, show it was a mixed feeder (Badgley et al., 2008). Baynunah bovids $\delta^{18}O$ values fall between those of the Siwaliks (more negative) and Lothagam (Fig. 18.11). One might interpret this as more mesic environments in the Siwaliks and more arid at Lothagam, but it could be the result of different source water values in each region.

Extant giraffids are represented by *Giraffa* and *Okapia*, both dedicated browsers. The Baynunah giraffids, in contrast, include the earliest evidence for C_4 grazing in a giraffid. Kingston (1999) previously discussed this observation, and here we add two additional sivathere specimens (AUH 204 and AUH 1124) that confirm that these early large giraffids had C_4-dominated diets. The median oxygen isotope value for the Baynunah sivatheres (+ 4.9 ‰) is 8 ‰ more positive than the median value for all other Baynunah large mammals (−3.1 ‰; Fig. 18.7), which indicates a major difference in physiology or water-use strategy from the other Baynunah large mammals, a pattern observed at other late Miocence sites (Domingo et al., 2017). One possible mechanism that would lead to the high $\delta^{18}O$ values is that these sivatheres may have ingested most of their water from evaporated leaf water or drank from an evaporated water source. The other sampled giraffid, tentatively assigned to *Paleotragus germaini* or cf. *Samotherium*, had a C_3-dominated diet, similar to those at Lothagam and in the Siwaliks (Fig. 18.11), but also had a very high $\delta^{18}O_{enamel}$ value. This suggests that the elevated $\delta^{18}O_{enamel}$ values

in giraffids, was dominated by plant water, as is observed in modern giraffes. All Baynunah giraffids come from the Ras Dubay'ah 2 (RDB 2) locality, which might also have been more arid relative to other contemporaneous sites. Equids from Ras Dubay'ah also show high oxygen isotope values relative to those from all other sites (difference of ~4.5 ‰), supporting this notion.

The Baynunah hippopotamid, *Archaeopotamus qeshta*, has the most C_4-rich diet of all the taxa sampled (Fig. 18.7). Extant *Hippopotamus* feeds along the banks or floodplains of aquatic systems, often on C_4 grasses and under the cover of night. Perhaps a similar scenario unfolded along the banks of the Baynunah river system. The Baynunah hippopotamids also exhibit the narrowest dietary range of all the Baynunah large mammals sampled, and narrower than the range exhibited by hippopotamids at other contemporaneous sites (Fig. 18.11). At both Lothagam and Toros-Menalla, hippopotamids maintained much wider dietary ranges and more mixed C_3-C_4 diets (Boisserie et al., 2005; Uno et al., 2011). Finally, we note that the Baynunah hippos exhibit the lowest $\delta^{18}O$ values of all fauna, more than 3 ‰ more negative than the median value of all non-hippo taxa, providing strong support for a semi aquatic lifestyle in early hippopotamines. The isotope date from the Baynunah hippos support the idea of the Hippopotamine Event around 8 Ma, which saw the diversification of hippopotamids into aquatic habitats and C_4 diets (Boisserie and Merceron, 2011).

The Suidae are the only Baynunah artiodactyl with a C_3-dominated diet. Only three samples representing two species, *Nyanzchoreus syrticus* and *Propotomochoerus hysudricus,* were analyzed but all fall squarely within the C_3 range. Coeval late Miocene suids from the Siwaliks, which also include the taxon *P. hysudricus*, were also almost all C_3 feeders (Badgley et al., 2008). In contrast, lower Nawata suids, comprised primarily of *Nyanzachoerus* spp., had

some C_3-dominated but mostly mixed diets (Uno et al., 2011; Fig. 18.11). Thus, although the Baynunah Suidae are taxonomically represented by an African and South Asian species each, their diets were more similar to their South Asian counterparts.

4.2.1.2. Perissodactyls

Equids are common in the Baynunah, with nearly 200 specimens recovered from multiple sites and they comprise over a third of the isotope data set. They are represented by at least two species, "*Hipparion*" *abudhabiense* and a second small "*Hipparion*" (Bernor et al., Ch. 16, this volume). Baynunah equids have a highly variable diet (24 to 84 $\%C_4$), with most sampled individuals falling into the mixed diet category. Median $\delta^{13}C$ values are similar to those of *S. emiratus* and *A. qeshta*. The intratooth profiles from six cheek teeth show that they had seasonally variable diets that ranged from 22 to 97 %C4 after taking enamel maturation and sampling geometry into consideration. The profiles suggest consumption of C_4 grasses was highest during the wet season, as indicated by a general inverse relationship between the carbon and oxygen intratooth profiles (Fig. 18.8).

The diet of the Baynunah equids falls between that of Siwaliks and Lothagam equids (Fig. 18.11). From 8 to 7 Ma, Siwaliks equids relied more on browsing (or C_3 grazing) than those in the Baynunah, whereas African equids were nearly all C_4 grazers by this time. In late Neogene fossil localities around the world, including East Africa, South Asia, and North America, equids serve as the "first responders" to C_4 vegetation on the landscape (Morgan and Kingston, 1994; Passey et al., 2002; Uno et al., 2011). Although tempting, it is not possible to estimate the age of the Baynunah fauna based on the amount of C_4 vegetation in their diets. The

timing of initiation and rate of spread of C_4 ecosystems varied significantly across continents from 10 to 3 Ma and as a result, the first indication of significant C_4 vegetation (>50%) in equid diets is also varied. It occurs in Africa at ~10 Ma, in the Siwaliks around 8.7 Ma, and in North America around 6.1 Ma (Badgley et al., 2008; Nelson, 2005; Passey et al., 2002; Uno et al., 2011).

Rhinocerotids are very rare in the Baynunah Formation. The two tooth fragments analyzed from Shuwaihat (SHU 1) indicate it was one of the few taxa that had a nearly pure C_3 diet. Both fragmentary specimens were found within a year of each other (1989 and 1990) at the same site and have similar carbon and oxygen values, so it is possible they represent the same individual. The diet of the Baynunah rhinocerotid(s) was similar to the browsing forms at Lothagam that included *Brachypotherium lewisi*, *Ceratotherium* sp., and *Diceros praecox* (Uno et al., 2011).

4.2.1.3. Proboscideans

The dominant proboscidean in the Baynunah, *Stegotetrabelodon emiratus*, had a mixed to C_4-dominated diet. Elephantidae and Gomphotheriidae from the Lower Nawata at Lothagam also had mixed C_3-C_4 diets, but by the Upper Nawata (~6.5 Ma) had all shifted to C_4-dominate diets (Fig. 18.11). The single gomphothere specimen from Baynunah had a diet that was broadly similar to *S. emiritus*, but with less C_4 (48 %C4) than its lower Nawata counterparts. Baynunah deinotheres, like those from Lothagam and specimens from the Siwaliks (> 8 Ma), had C_3-dominated diets.

4.2.1.4. Baynunah Dietary Structure

It is interesting that the giraffids, hippopotamids, equids, and elephantids, which together account for 80 % of the samples analyzed, show such large overlap in their diets based on the carbon isotope data (Fig. 18.7). From a carbon isotope perspective, this shows significant overlap in their dietary niches. Intratooth carbon isotope profiles reveal that the equids had seasonally variable diets, and the range of carbon isotope values in elephants suggests this may have been the case there too (Fig. 18.6). In contrast, the narrow range of hippopotamid values suggests their diets were less variable throughout the year. The giraffids occupied both grazing and mixed feeding to browsing niches, but it is not clear if seasonal variations in diet may have been present. Additional intratooth profiles would be useful in this regard. What is clear is the strong separation between the C_3-dependent (browsing) clades— deinotheriids, suids, and rhinocerotids —and the mixed feeding to graze-dominated giraffids, bovids, hippopotamids, proboscideans, and equids (Fig. 18.6). The three browsers are all very rare in terms of number of identified specimens, while the mixed-feeding to grazing ungulates (particularly equids and hippopotamids) are far more abundant (Bibi et al., Ch. 19, this volume). This suggests that, while tree cover and browsing taxa were present in the Baynunah, the landscape was likely a woody grassland, as pedogenic carbonate and plant wax $\delta^{13}C$ values also indicate.

The dietary structure of Baynunah large mammals is more similar to Lothagam than the Siwaliks. The former sites are dominated by mixed feeding to graze-dominated herbivores whereas the Siwaliks at that time still had large C_3-dominated (browsing) herbivores, represented by the suids and bovids, and some mixed feeders. Equid intratooth profiles from Baynunah and the Siwaliks indicate that in both regions a monsoon system exerted primary control of

hydroclimate. The seasonality of precipitation was stronger at Baynunah based on the intratooth amplitude of $\delta^{18}O$. Intratooth profiles from coeval African fauna could help constrain seasonality there during the late Miocene.

5. Conclusions

Our findings indicate C_4 grasses were an important part of Baynunah ecosystems, and at an age of around 7 Ma, the Baynunah represents one of the earliest woody grasslands, or mixed C_3-C_4 to C_4-dominated ecosystems, known to date. The strong reliance of the most abundant large mammal clades on C_4-feeding, even if only seasonally, indicates large mammals were already well-adapted to (and almost certainly co-evolved with) C_4 grasses by this time. The strong, monsoonal-type rainfall seasonality revealed by the equid intratooth isotope profiles describe an ideal environment for the proliferation of C_4 grasses.

The dominance of grasses however did not preclude the presence of woody vegetation and cover, as at least one giraffid, two suids, a deinotherid, and a rhinocerotid subsisted entirely on C_3 resources, most likely browse. The resulting 'mosaic' of grasslands and trees is typical for the diversity of environments referred to as savannas, today characteristic of sub-Saharan Africa, but widespread across Afro-Arabia and large tracts of Eurasia during the late Miocene, (Fortelius et al., 2002; Kaya et al., 2018).

Acknowledgements

This work was supported by the Abu Dhabi Department of Culture and Tourism (formerly TCA, formerly ADACH) and the US National Science Foundation (grants OISE-0852975 to FB, and 0321893 - RHOI - to T. White and F. C. Howell). We acknowledge and thank the many scientists who conducted field work and lab work to build the collection of fossil teeth sampled in this study and who identified and described the outcrops where sediments were sampled for compound specific isotope analyses of plant waxes. We thank Mark Franklin and Natalia Galud Erazo for assistance with sampling, pretreatment, and weighing of enamel samples for isotope analysis and Wei Huang for assistance with mass spectrometry. We also thank Gertrud Rössner and the BSPG (Munich) for providing an enamel sample of BSPG 1965 I112. We thank Drs. Laura Domingo and Naomi Levin for thorough reviews which helped improve the manuscript. KTU thanks Michelle Morgan and Sherry Nelson for providing published Siwaliks enamel isotope data in electronic format and John Kingston for providing Baynunah enamel and pedogenic carbonate isotope data in electronic format. This is Lamont-Doherty Earth Observatory contribution #8XXX.

Figures: 1 through 9

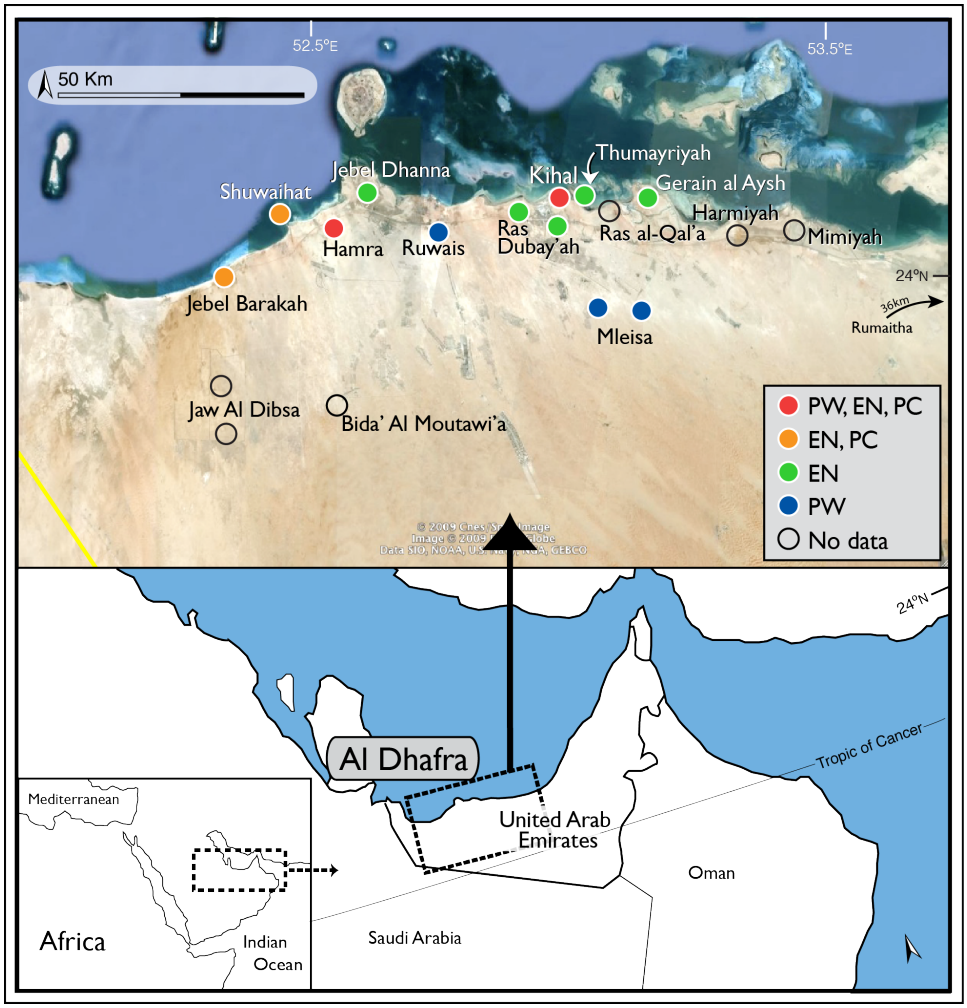

Figure 18.1. Location of Baynunah Formation localities (circles) in the Al Dhafra region, western Abu Dhabi Emirate, United Arab Emirates. Sites are coded by color based on isotopic sample type (PW, plant wax; EN, enamel; PC, pedogenic carbonate). Modified from (Bibi et al., 2013).
[1.5 column width]

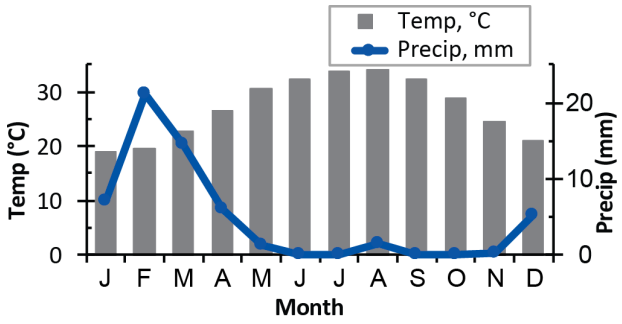

Figure 18.2. Modern monthly temperature (gray bars) and precipitation (blue line) of Abu Dhabi from 1971 to 1991 (NOAA, 2018). [single column width]

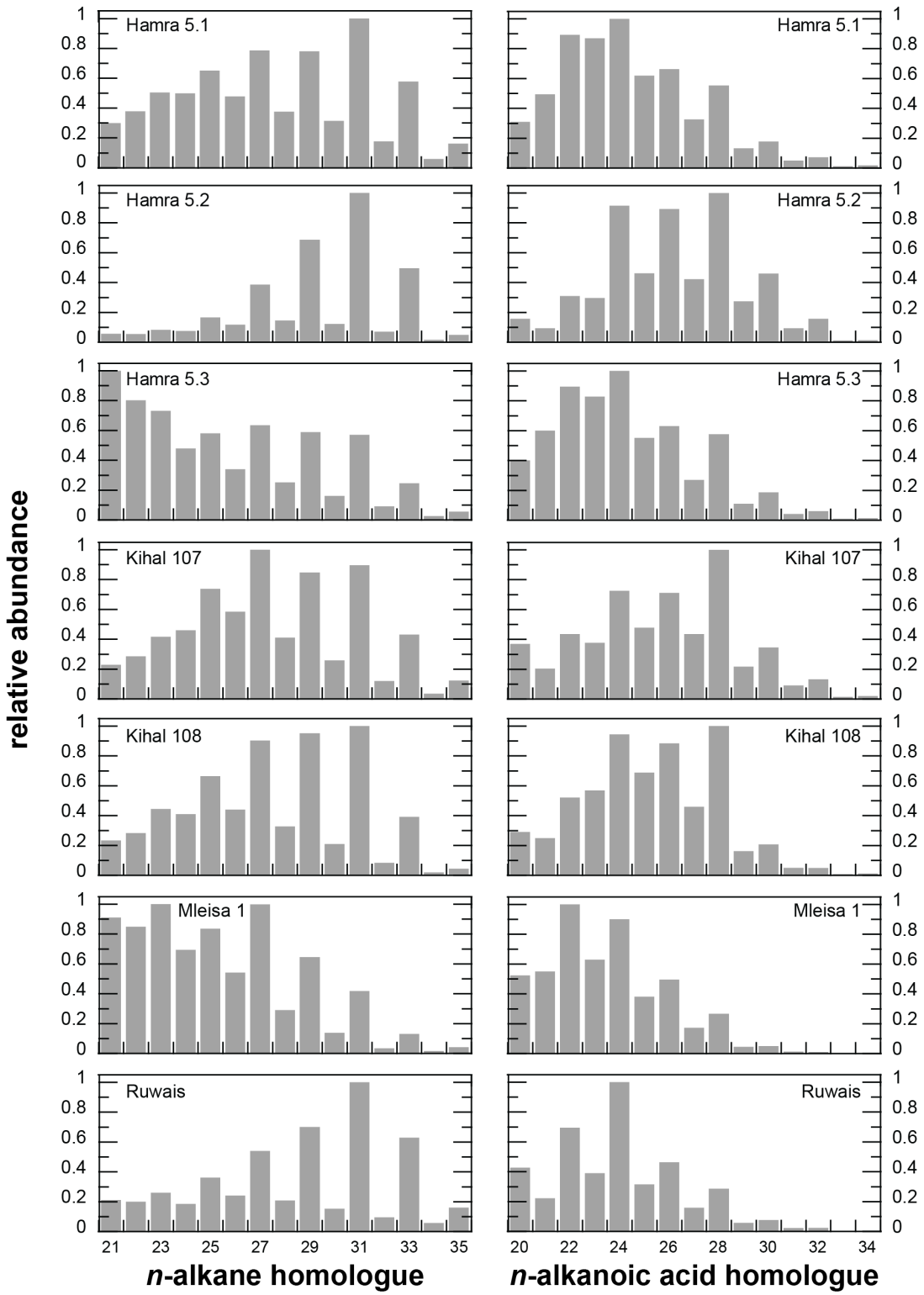

Figure 18.3. Normalized plant wax concentrations for *n*-alkanes and *n*-alkanoic acids at different sites of the Baynunah Formation (all contemporaneous). [full page]

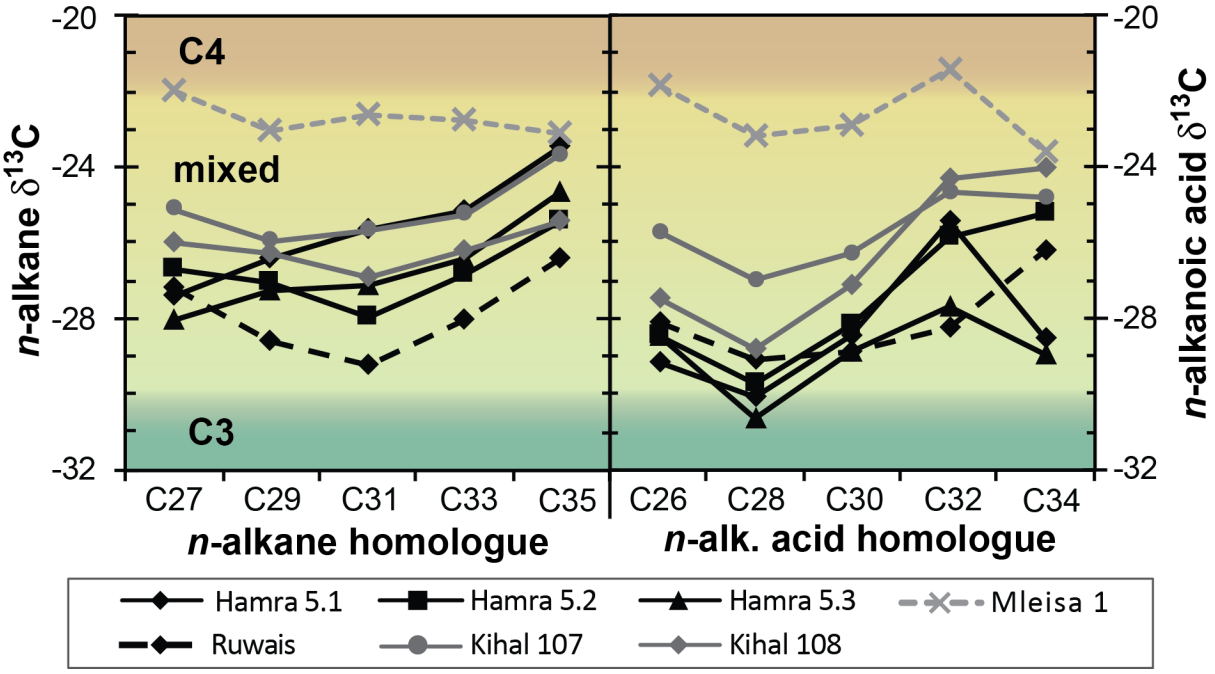

Figure 18.4. Plant wax $\delta^{13}C$ values for *n*-alkanes and *n*-alkanoic acids (‰, VPDB). [full page width]

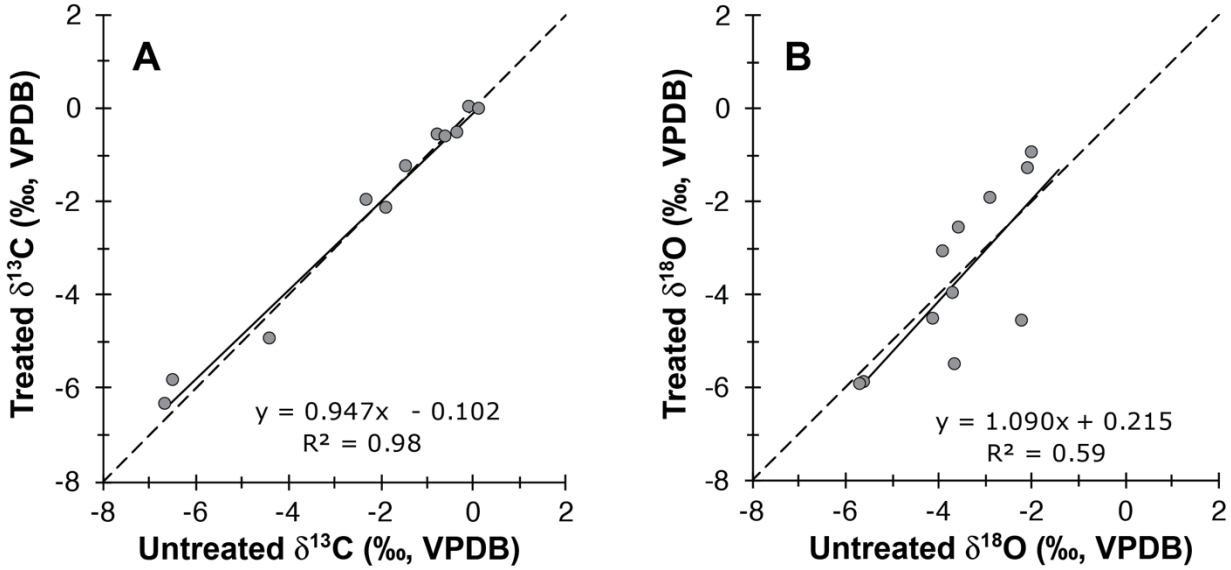

Figure 18.5. Cross-plot of carbon and oxygen isotope values for treated vs untreated tooth enamel (‰, VPDB). [full page width]

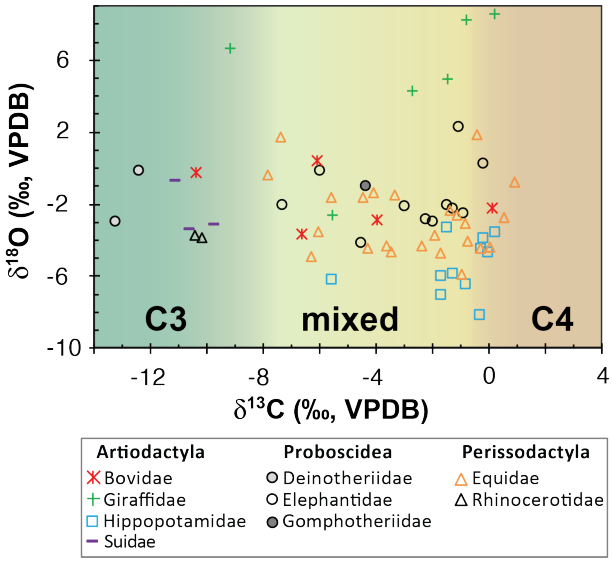

Figure 18.6. Cross-plot of fossil enamel carbon and oxygen isotope values (‰, VPDB) for nine mammalian families. Data include isotope values from Kingston (1999). [single column width]

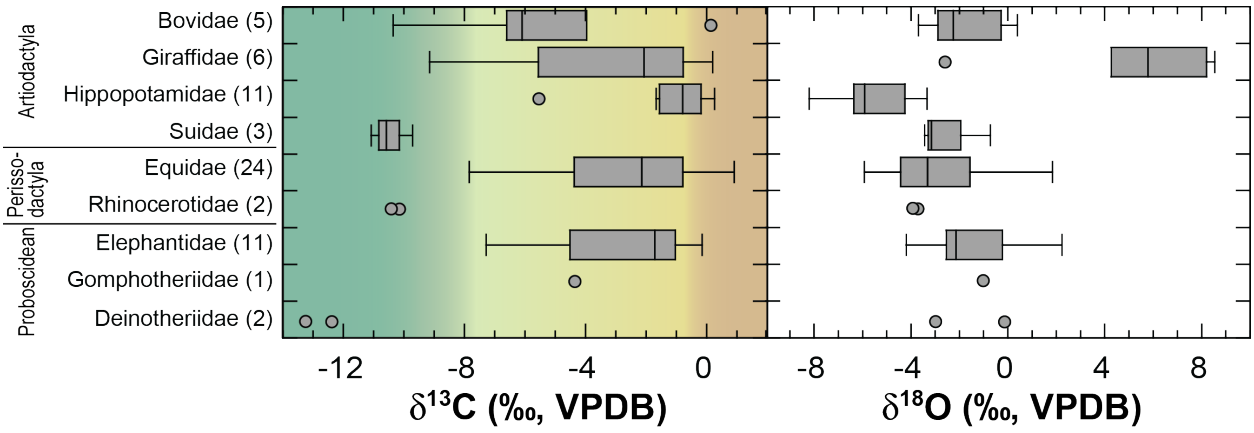

Figure 18.7. Carbon and oxygen isotope box plots by family. Carbon isotope data show that most taxa are mixed feeders but hippos are grazers and suids, rhinocerotids, and deinotherids are browsers. For oxygen isotopes, hippopotamid values are low, as expected for semi-aquatic habits, whereas giraffid values are high, indicating strong evaporative effects on plant water, evaporated drinking water, or a combination of both. Data include isotope values from Kingston (1999). [full page width]

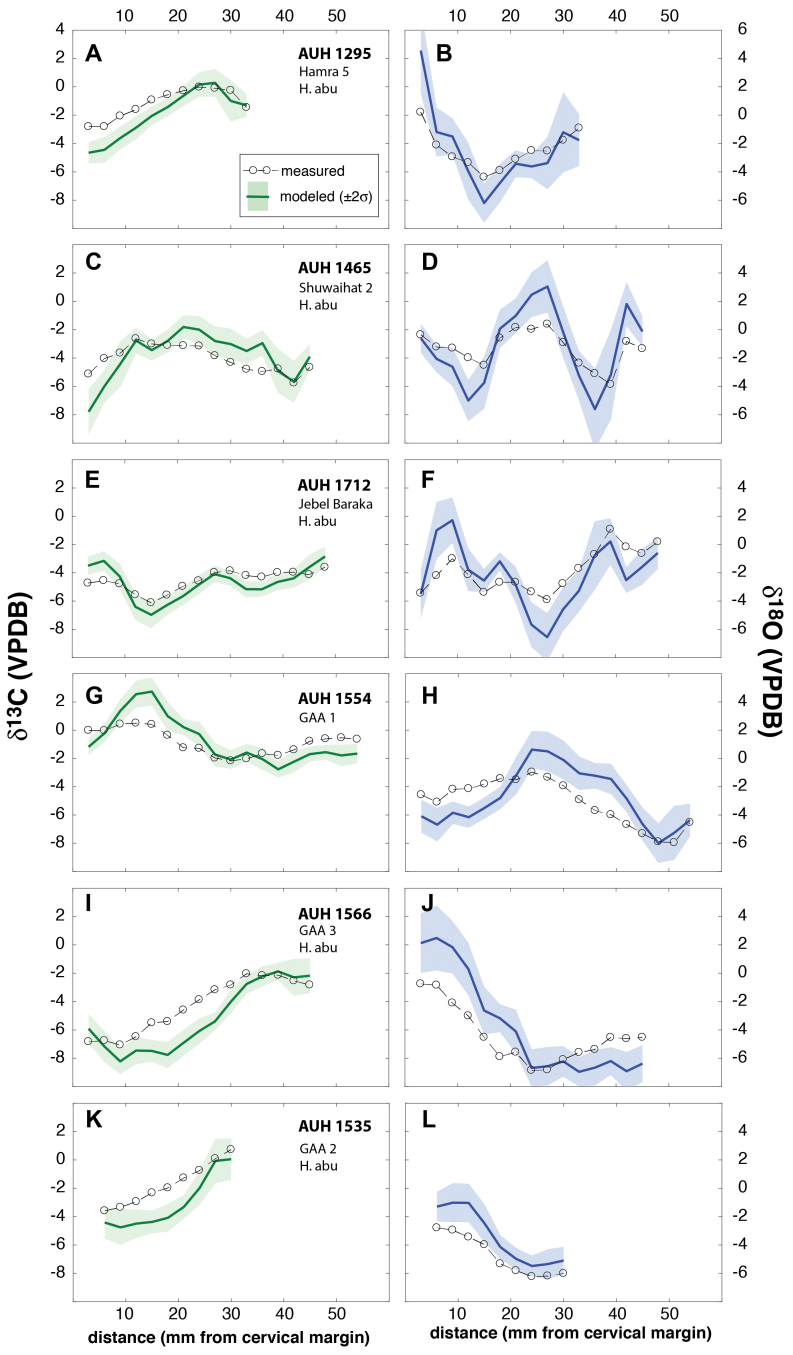

Figure 18.8. Equid intratooth isotope profiles of carbon (left column) and corresponding oxygen isotope values (right column). In general, carbon and oxygen data covary out of phase with one another. H abu. is "*Hipparion*" *abudhabiense*. Open circles are smoothed measured values, lines represent modeled values, and shaded areas represent ±2σ of modeled values. [full page]

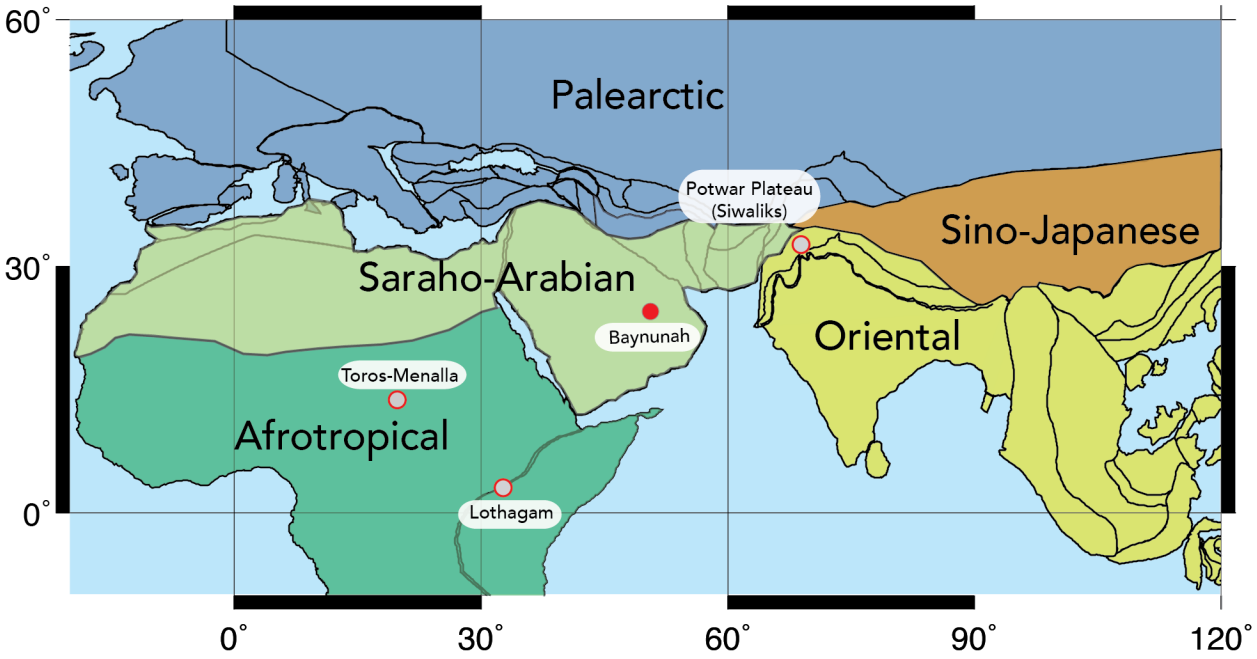

Figure 18.9. Late Miocene vertebrate fossil sites where large stable isotope data sets are available. Paleogeography is based on a 7 Ma plate reconstruction using the Ocean Drilling Stratigraphic Network's Plate Tectonic Reconstruction Service (http://www.odsn.de/odsn/services/paleomap/paleomap.html) and modern zoogeographic zones are from Holt et al.(2013). [full page width]

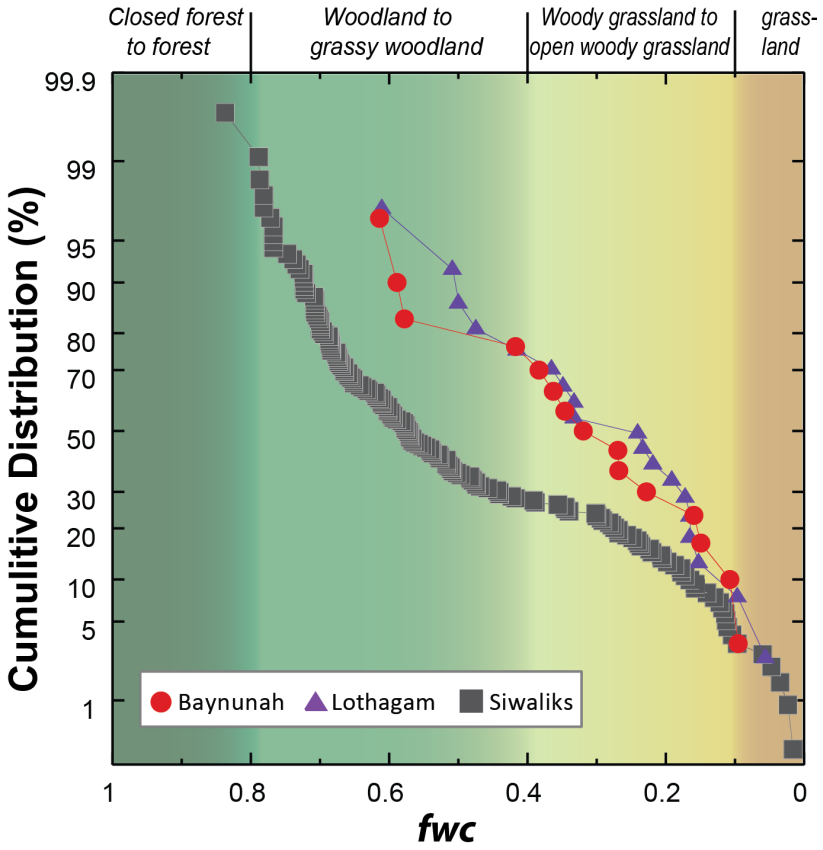

Figure 18.10. Cumulative distribution of fraction woody cover (*fwc*) data derived from $\delta^{13}C$ values of pedogenic carbonates from Baynunah (red circles), Lothagam (purple triangles), and the Siwaliks (gray squares) from 8-6 Ma. Data are from Cerling et al., 2003a; Kingston, 1999; and Behrensmeyer et al., 2007. [single column width]

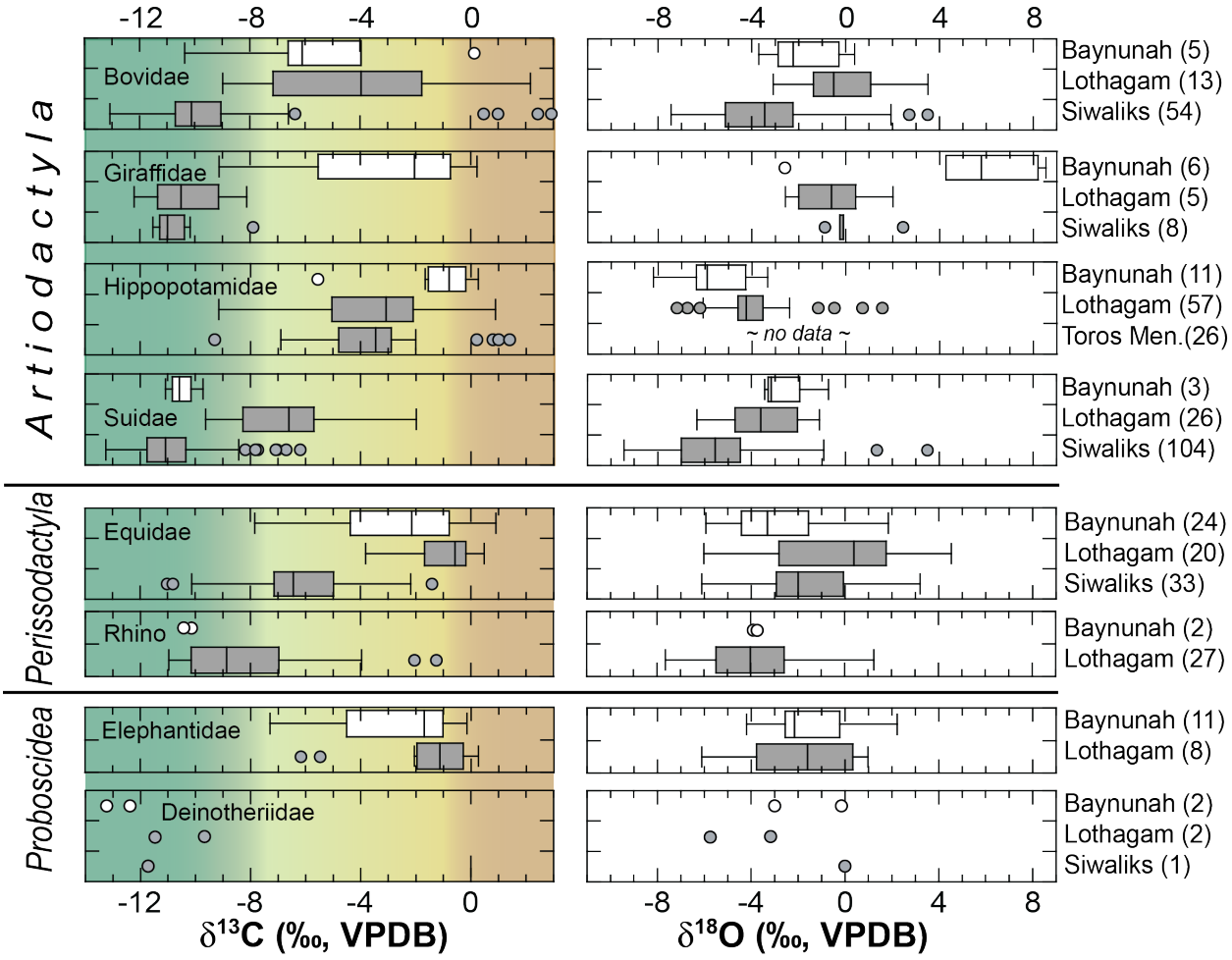

Figure 18.11. Box plots of Baynunah (white), Lothagam (gray; Nawata Formation), Siwaliks (gray; late Miocene (8-6 Ma) data only), and Toros Menalla (gray) carbon and oxygen isotope data from fossil enamel (Badgley et al., 2008; Boisserie et al., 2005; Cerling et al., 2003a; Kingston, 1999; Uno et al., 2011). [full page width]

Tables 18.1 through 18.9.
See Excel file: Baynunah manuscript data.xlsx

Table 18.1. Calculated $\delta^{13}C$ values (‰,VPDB) for paleosol carbonate, enamel, and plant waxes formed in equilibrium with C_3 and C_4 vegetation. The $\delta^{13}C$ values of atmospheric CO_2 are from the high resolution benthic foramanifera record in Tipple et al. (2010).

Table 18.2. Plant wax sample information including lithology, concentrations, and CPI and ACL values.

Table 18.3. Carbon isotope data (‰,VPDB) for odd-chain *n*-alkanes (C_{27} to C_{35}) and even-chain fatty acids (C_{26} to C_{34}). Percent C_4 vegetation is calculated from the *n*-C_{31} alkane where uncertainty, given as 1σ, accounts for C_3 and C_4 endmember variability and analytical uncertainty.

Table 18.4. Comparison of tooth enamel carbon and oxygen isotope data from treated and untreated equid tooth samples (‰,VPDB).

Table 18.5. Tooth enamel carbon and oxygen isotope data for Baynunah large mammals (‰,VPDB). Percent C_4 diet is given along with uncertainty (1σ) that accounts for C_3 and C_4 endmember variability and analytical uncertainty. Data include carbon and oxygen values from Kingston, 1999. The original oxygen isotope values from Kingston are also provided (K99).

Table 18.6. Intratooth stable isotope (‰,VPDB) and %C4 (± 1σ) data for equid molar profiles. Smoothed data (3 pt., weighted 0.25/0.50/0.25) and inverse model results (estimated input signal) are given with 2σ uncertainty. Sample locations are given as distance from the cervix. Summary statistics are provided for each intratooth profile. Estimated input signal was calculated using Matlab code modified from "mSolve_1.m" published by Passey et al. (2005).

Table 18.7. Modern $\delta^{18}O$ values (‰,VSMOW) for precipitation include measured values from the United Arab Emirates (UAE) and Bahrain and modeled values for western Abu Dhabi based on the Online Isotopes in Precipitation Calculator (OIPC).

Table 18.8. Summary statistics of percent C_4 vegetation and diet at different Baynunah Formation fossil sites. Median uncertainty in percent C_4 calculations is ±12%.

Table 18.9. Fraction woody cover (fwc) data calculated from pedogenic carbonate $\delta^{13}C$ values from Baynunah, Lothagam, and the Pakistani Siwaliks. Data from the latter two sites are restricted to 8 to 6 Ma and all paleomagnetic based ages for the Siwaliks were updated to the timescale of Gradstein and Ogg (2012). Data are from Kingston (1999), Cerling et al. (2003a), Quade et al. (1989), and Behrensmeyer et al. (2007).

References Cited

2015, Global Network of Isotopes in Precipitation.

Baczynski, A. A., McInerney, F. A., Wing, S. L., Kraus, M. J., Morse, P. E., Bloch, J. I., Chung, A. H., and Freeman, K. H., 2016, Distortion of carbon isotope excursion in bulk soil organic matter during the Paleocene-Eocene thermal maximum: Geological Society of America Bulletin, v. 128, no. 9-10, p. 1352-1366.

Badgley, C., Barry, J. C., Morgan, M. E., Nelson, S. V., Behrensmeyer, A. K., Cerling, T. E., and Pilbeam, D., 2008, Ecological changes in Miocene mammalian record show impact of prolonged climatic forcing: Proceedings of the National Academy of Sciences, v. 105, no. 34, p. 12145-12149.

Barry, J. C., Morgan, M. E., Flynn, L. J., Pilbeam, D., Behrensmeyer, A. K., Raza, S. M., Khan, I. A., Badgley, C., Hicks, J., and Kelley, J., 2002, Faunal and environmental change in the late Miocene Siwaliks of northern Pakistan: Paleobiology, v. 28, no. S2, p. 1-71.

Behrensmeyer, A. K., Quade, J., Cerling, T. E., Kappelman, J., Khan, I. A., Copeland, P., Roe, L., Hicks, J., Stubblefield, P., Willis, B. J., and Latorre, C., 2007, The structure and rate of late Miocene expansion of C4 plants: Evidence from lateral variation in stable isotopes in paleosols of the Siwalik Group, northern Pakistan: Geological Society of America Bulletin, v. 119, no. 11-12, p. 1486-1505.

Bendrey, R., Vella, D., Zazzo, A., Balasse, M., and Lepetz, S., 2015, Exponentially decreasing tooth growth rate in horse teeth: implications for isotopic analyses: Archaeometry, v. 57, no. 6, p. 1104-1124.

Bibi, F., Hill, A., Beech, M., and Yasin, W., 2013, Late Miocene Fossils from the Baynunah Formation, United Arab Emirates, *in* Wang, X., Flynn, L. J., and Fortelius, M., eds., Fossil Mammals of Asia: Neogene Biostratigraphy and Chronology: New York, Columbia University Press p. 583-594.

Bibi, F., Kraatz, B., Craig, N., Beech, M., Schuster, M., and Hill, A., 2012, Early evidence for complex social structure in Proboscidea from a late Miocene trackway site in the United Arab Emirates: Biol Lett, v. 8, no. 4, p. 670-673.

Blumenthal, S. A., Cerling, T. E., Chritz, K. L., Bromage, T. G., Kozdon, R., and Valley, J. W., 2014, Stable isotope time-series in mammalian teeth: in situ δ 18 O from the innermost enamel layer: Geochimica et Cosmochimica Acta, v. 124, p. 223-236.

Bocherens, H., Koch, P., Mariotti, A., Geraads, D., and Jaeger, J., 1996, Isotopic biogeochemistry (13 C, 18 O) of mammalian enamel from African Pleistocene hominid sites: Palaios, v. 11, no. 4, p. 306-318.

Boisserie, J.-R., and Merceron, G., 2011, Correlating the success of Hippopotaminae with the C4 grass expansion in Africa: Relationship and diet of early Pliocene hippopotamids from Langebaanweg, South Africa: Palaeogeography, Palaeoclimatology, Palaeoecology, v. 308, no. 3-4, p. 350-361.

Boisserie, J.-R., Zazzo, A., Merceron, G., Blondel, C., Vignaud, P., Likius, A., Mackaye, H. T., and Brunet, M., 2005, Diets of modern and late Miocene hippopotamids: Evidence from

carbon isotope composition and micro-wear of tooth enamel: Palaeogeography, Palaeoclimatology, Palaeoecology, v. 221, no. 1-2, p. 153-174.
Bowen, G. J., 2018, The Online Isotopes in Precipitation Calculator, version 3.1.
Bowen, G. J., and Revenaugh, J., 2003, Interpolating the isotopic composition of modern meteoric precipitation: Water Resources Research, v. 39, no. 10.
Bryant, J. D., Koch, P. L., Froelich, P. N., Showers, W. J., and Genna, B. J., 1996, Oxygen isotope partitioning between phosphate and carbonate in mammalian apatite: Geochimica et Cosmochimica Acta, v. 60, no. 24, p. 5145-5148.
Bush, R. T., and McInerney, F. A., 2013, Leaf wax n-alkane distributions in and across modern plants: Implications for paleoecology and chemotaxonomy: Geochimica et Cosmochimica Acta, v. 117, p. 161-179.
-, 2015, Influence of temperature and C 4 abundance on n-alkane chain length distributions across the central USA: Organic Geochemistry, v. 79, p. 65-73.
Cerling, T., and Harris, J., 1999, Carbon isotope fractionation between diet and bioapatite in ungulate mammals and implications for ecological and paleoecological studies: Oecologia, v. 120, no. 3, p. 347-363.
Cerling, T., Harris, J., and Leakey, M., 2003a, Isotope paleoecology of the Nawata and Nachukui Formations at Lothagam, Turkana Basin, Kenya, *in* Leakey, M. G., and Harris, J. M., eds., Lothagam: The Dawn of Humanity in Eastern Africa: New York, Columbia University Press, p. 605-623.
Cerling, T., Harris, J., Leakey, M., and Mudidia, N., 2003b, Stable isotope ecology of Northern Kenya, with emphasis on the Turkana Basin, *in* Leakey, M. G., and Harris, J. M., eds., Lothagam: The Dawn of Humanity in Eastern Africa: New York, Columbia University Press, p. 583-603.
Cerling, T. E., Harris, J. M., Hart, J. A., Kaleme, P., Klingel, H., Leakey, M. G., Levin, N. E., Lewison, R. L., and Passey, B. H., 2008, Stable isotope ecology of the common hippopotamus: Journal of Zoology, v. 276, no. 2, p. 204-212.
Cerling, T. E., Wynn, J. G., Andanje, S. A., Bird, M. I., Korir, D. K., Levin, N. E., Mace, W., Macharia, A. N., Quade, J., and Remien, C. H., 2011, Woody cover and hominin environments in the past 6 million years: Nature, v. 476, no. 7358, p. 51-56.
Collister, J. W., Rieley, G., Stern, B., Eglinton, G., and Fry, B., 1994, Compound-specific $\delta^{13}C$ analyses of leaf lipids from plants with differing carbon dioxide metabolisms: Organic Geochemistry, v. 21, no. 6, p. 619-627.
Corrigan, D., Kloos, C., O'Connor, C. S., and Timoney, R. F., 1973, Alkanes from four species of Sphagnum moss: Phytochemistry, v. 12, no. 1, p. 213-214.
Cranwell, P. A., Eglinton, G., and Robinson, N., 1987, Lipids of aquatic organisms as potential contributors to lacustrine sediments—II: Organic Geochemistry, v. 11, no. 6, p. 513-527.
Crowell-Davis, S. L., Houpt, K. A., and Carnevale, J., 1985, Feeding and drinking behavior of mares and foals with free access to pasture and water: Journal of animal science, v. 60, no. 4, p. 883-889.
Dansgaard, W., 1964, Stable isotopes in precipitation: Tellus, v. 16, no. 4, p. 436-468.

Domingo, L., Domingo, M. S., Koch, P. L., Morales, J., and Alberdi, M. T., 2017, Carnivoran resource and habitat use in the context of a Late Miocene faunal turnover episode: Palaeontology, v. 60, no. 4, p. 461-483.
Eglinton, G., and Hamilton, R. J., 1967, Leaf Epicuticular Waxes: Science, v. 156, no. 3780, p. 1322-1335.
Feakins, S. J., deMenocal, P. B., and Eglinton, T. I., 2005, Biomarker records of late Neogene changes in northeast African vegetation: Geology, v. 33, no. 12, p. 977-980.
Feakins, S. J., Levin, N. E., Liddy, H. M., Sieracki, A., Eglinton, T. I., and Bonnefille, R., 2013, Northeast African vegetation change over 12 my: Geology, v. 41, no. 3, p. 295-298.
Ficken, K. J., Li, B., Swain, D. L., and Eglinton, G., 2000, An n-alkane proxy for the sedimentary input of submerged/floating freshwater aquatic macrophytes: Organic Geochemistry, v. 31, no. 7, p. 745-749.
Fortelius, M., Eronen, J., Jernvall, J., Liu, L., Pushkina, D., Rinne, J., Tesakov, A., Vislobokova, I., Zhang, Z., and Zhou, L., 2002, Fossil mammals resolve regional patterns of Eurasian climate change over 20 million years: Evolutionary Ecology Research, v. 4, no. 7, p. 1005-1016.
Fortelius, M., Žliobaitė, I., Kaya, F., Bibi, F., Bobe, R., Leakey, L., Leakey, M., Patterson, D., Rannikko, J., and Werdelin, L., 2016, An ecometric analysis of the fossil mammal record of the Turkana Basin: Philosophical Transactions of the Royal Society of London B: Biological Sciences, v. 371, no. 1698.
Freeman, K. H., and Colarusso, L. A., 2001, Molecular and isotopic records of C4 grassland expansion in the late miocene: Geochimica et Cosmochimica Acta, v. 65, no. 9, p. 1439-1454.
Freeman, K. H., Hayes, J. M., Trendel, J. M., and Albrecht, P., 1990, Evidence from carbon isotope measurements for diverse origins of sedimentary hydrocarbons: Nature (London), v. 343, no. 6255, p. 254-256.
Fricke, H. C., and O'Neil, J. R., 1996, Inter-and intra-tooth variation in the oxygen isotope composition of mammalian tooth enamel phosphate: implications for palaeoclimatological and palaeobiological research: Palaeogeography, Palaeoclimatology, Palaeoecology, v. 126, no. 1, p. 91-99.
Friend, P., 1999, Rivers of the Lower Baynunah Formation, Emirate of Abu Dhabi, United Arab Emirates, *in* Whybrow, P. J., and Hill, A., eds., Fossil Vertebrates of Arabia: New Haven, Connecticut, Yale University Press,, p. 38-49.
Good, S. P., and Caylor, K. K., 2011, Climatological determinants of woody cover in Africa: Proc Natl Acad Sci U S A, v. 108, no. 12, p. 4902-4907.
Hailwood, E. A., and Whybrow, P. J., 1999, Paleomagnetic correlation and dating of the Baynunah and Shuwaihat Formations, *in* Whybrow, P. J., and Hill, A., eds., Fossil Vertebrates of Arabia: New Haven, Connecticut, Yale University Press,, p. 28-37.
Hayes, J. M., Freeman, K. H., Popp, B. N., and Hoham, C. H., 1990, Compound-specific isotopic analyses; a novel tool for reconstruction of ancient biogeochemical processes: Organic Geochemistry, v. 16, no. 4-6, p. 1115-1128.
Hill, A., Whybrow, P. J., and Yasin, W., 1999, History of Paleontological Research in the Western Region of the Emirate of Abu Dhabi, United Arab Emirates, *in* Whybrow, P. J., and Hill,

A., eds., Fossil Vertebrates of Arabia: New Haven, Connecticut, Yale University Press, p. 18-23.
Holt, B. G., Lessard, J.-P., Borregaard, M. K., Fritz, S. A., Araújo, M. B., Dimitrov, D., Fabre, P.-H., Graham, C. H., Graves, G. R., and Jønsson, K. A., 2013, An update of Wallace's zoogeographic regions of the world: Science, v. 339, no. 6115, p. 74-78.
Hoppe, K. A., Stover, S. M., Pascoe, J. R., and Amundson, R., 2004, Tooth enamel biomineralization in extant horses: implications for isotopic microsampling: Palaeogeography, Palaeoclimatology, Palaeoecology, v. 206, no. 3-4, p. 355-365.
Huang, Y., Clemens, S. C., Liu, W., Wang, Y., and Prell, W. L., 2007, Large-scale hydrological change drove the late Miocene C4 plant expansion in the Himalayan foreland and Arabian Peninsula: Geology, v. 35, no. 6, p. 531-534.
Huertas, A. D., Iacumin, P., Stenni, B., Chillón, B. S., and Longinelli, A., 1995, Oxygen isotope variations of phosphate in mammalian bone and tooth enamel: Geochimica et Cosmochimica Acta, v. 59, no. 20, p. 4299-4305.
Jennings, R. P., Singarayer, J., Stone, E. J., Krebs-Kanzow, U., Khon, V., Nisancioglu, K. H., Pfeiffer, M., Zhang, X., Parker, A., and Parton, A., 2015, The greening of Arabia: Multiple opportunities for human occupation of the Arabian Peninsula during the Late Pleistocene inferred from an ensemble of climate model simulations: Quaternary International, v. 382, p. 181-199.
Kaya, F., Bibi, F., Žliobaitė, I., Eronen, J. T., Hui, T., and Fortelius, M., 2018, The rise and fall of the Old World savannah fauna and the origins of the African savannah biome: Nature ecology & evolution, v. 2, no. 2, p. 241.
Kim, S. T., and O'Neil, J. R., 1997, Equilibrium and nonequilibrium oxygen isotope effects in synthetic carbonates: Geochimica et Cosmochimica Acta, v. 61, no. 16, p. 3461-3475.
Kingston, J. D., 1999, Isotopes and environments of the Baynunal Formation, Emirate of Abu Dhabi, United Arab Emirates, *in* Whybrow, P. J., and Hill, A., eds., Fossil Vertebrates of Arabia: New Haven, CT, Yale University Press, p. 354-372.
Kingston, J. D., and Harrison, T., 2007, Isotopic dietary reconstructions of Pliocene herbivores at Laetoli: Implications for early hominin paleoecology: Palaeogeography, Palaeoclimatology, Palaeoecology, v. 243, no. 3-4, p. 272-306.
Kohn, M. J., Schoeninger, M. J., and Valley, J. W., 1996, Herbivore tooth oxygen isotope compositions: effects of diet and physiology: Geochimica et Cosmochimica Acta, v. 60, no. 20, p. 3889-3896.
Leakey, M., and Harris, J., 2003, Lothagam: The Dawn of Humanity in Eastern Africa, Columbia Univ Press.
Levin, N. E., Cerling, T. E., Passey, B. H., Harris, J. M., and Ehleringer, J. R., 2006, A stable isotope aridity index for terrestrial environments: Proceedings of the National Academy of Sciences of the United States of America, v. 93, no. 30, p. 11201-11205.
Livingstone, D., and Clayton, W., 1980, An altitudinal cline in tropical African grass floras and its paleoecological significance: Quaternary Research, v. 13, no. 3, p. 392-402.
Luz, B., Kolodny, Y., and Horowitz, M., 1984, Fractionation of oxygen isotopes between mammalian bone-phosphate and environmental drinking water: Geochimica et Cosmochimica Acta, v. 48, no. 8, p. 1689-1693.

Metcalfe, J. Z., Longstaffe, F. J., Ballenger, J. A. M., and Haynes Jr, C. V., 2011, Isotopic paleoecology of Clovis mammoths from Arizona: Proceedings of the National Academy of Sciences, v. 108, no. 44, p. 17916-17920.

Morgan, M., and Kingston, J., 1994, Carbon isotopic evidence for the emergence of C4 plants in the Neogene from Pakistan and Kenya: Nature, v. 367, p. 162-165.

Mueller, K. E., Polissar, P. J., Oleksyn, J., and Freeman, K. H., 2012, Differentiating temperate tree species and their organs using lipid biomarkers in leaves, roots and soil: Organic Geochemistry.

Nelson, S. V., 2005, Paleoseasonality inferred from equid teeth and intra-tooth isotopic variability: Palaeogeography, Palaeoclimatology, Palaeoecology, v. 222, no. 1, p. 122-144.

NOAA, 2018, NNDC Climatic Data OnLine, *in* Information, N. C. f. E., ed., NOAA.

Nott, C. J., Xie, S., Avsejs, L. A., Maddy, D., Chambers, F. M., and Evershed, R. P., 2000, n-Alkane distributions in ombrotrophic mires as indicators of vegetation change related to climatic variation: Organic Geochemistry, v. 31, no. 2-3, p. 231-235.

Passey, B. H., and Cerling, T. E., 2002, Tooth enamel mineralization in ungulates; implications for recovering a primary isotopic time-series: Geochimica et Cosmochimica Acta, v. 66, no. 18, p. 3225-3234.

Passey, B. H., Cerling, T. E., and Levin, N. E., 2007, Temperature dependence of oxygen isotope acid fractionation for modern and fossil tooth enamels: Rapid communications in mass spectrometry, v. 21, no. 17, p. 2853-2859.

Passey, B. H., Cerling, T. E., Perkins, M. E., Voorhies, M. R., Harris, J. M., and Tucker, S. T., 2002, Environmental change in the Great Plains; an isotopic record from fossil horses: Journal of Geology, v. 110, no. 2, p. 123-140.

Passey, B. H., Cerling, T. E., Schuster, G. T., Robinson, T. F., Roeder, B. L., and Krueger, S. K., 2005, Inverse methods for estimating primary input signals from time-averaged isotope profiles: Geochimica et Cosmochimica Acta, v. 69, no. 16, p. 4101-4116.

Passey, B. H., Levin, N. E., Cerling, T. E., Brown, F. H., and Eiler, J. M., 2010, High-temperature environments of human evolution in East Africa based on bond ordering in paleosol carbonates: Proceedings of the National Academy of Sciences, v. 107, no. 25, p. 11245.

Polissar, P. J., and D'Andrea, W. J., 2014, Uncertainty in paleohydrologic reconstructions from molecular δD values: Geochimica et Cosmochimica Acta, v. 129, p. 146-156.

Polissar, P. J., Rose, C., Uno, K. T., Phelps, S. R., and deMenocal, P., 2019, Synchronous rise of African C4 ecosystems 10 million years ago in the absence of aridification: Nature Geoscience, v. 12, no. 8, p. 657-660.

Popov, S. V., Rögl, F., Rozanov, A. Y., Steininger, F. F., Shcherba, I. G., and Kovac, M., 2004, Lithological-Paleogeographic maps of Paratethys-10 maps Late Eocene to Pliocene: Courier Forschungsinstitut Senckenberg, v. 250, p. 1-46.

Quade, J., Cerling, T. E., and Bowman, J. R., 1989, Development of Asian monsoon revealed by marked ecological shift during the latest Miocene in northern Pakistan: Nature (London), v. 342, no. 6246, p. 163-166.

Quade, J., Eiler, J., Daeron, M., and Achyuthan, H., 2013, The clumped isotope geothermometer in soil and paleosol carbonate: Geochimica et Cosmochimica Acta, v. 105, p. 92-107.

Sankaran, M., Hanan, N. P., Scholes, R. J., Ratnam, J., Augustine, D. J., Cade, B. S., Gignoux, J., Higgins, S. I., Le Roux, X., Ludwig, F., Ardo, J., Banyikwa, F., Bronn, A., Bucini, G., Caylor, K. K., Coughenour, M. B., Diouf, A., Ekaya, W., Feral, C. J., February, E. C., Frost, P. G. H., Hiernaux, P., Hrabar, H., Metzger, K. L., Prins, H. H. T., Ringrose, S., Sea, W., Tews, J., Worden, J., and Zambatis, N., 2005, Determinants of woody cover in African savannas: Nature, v. 438, no. 7069, p. 846-849.

Sharp, Z. D., Cerling, T. E., Cerling, T. E., Harris, J. M., and MacFadden, B. J., 1998, Fossil isotope records of seasonal climate and ecology; straight from the horse's mouth: Carbon isotopes, diets of North American equids, and the evolution of North American C4 grasslands: Geology, v. 26, no. 3, p. 219-222.

Suga, S., 1979, Comparative Histology of Progressive Mineralization Pattern of Developing Incisor Enamel of Rodents: Journal of Dental Research, v. 58, no. 2 suppl, p. 1025-1026.

Swart, P. K., Burns, S. J., and Leder, J. J., 1991, Fractionation of the stable isotopes of oxygen and carbon in carbon dioxide during the reaction of calcite with phosphoric acid as a function of temperature and technique: Chemical Geology: Isotope Geoscience section, v. 86, no. 2, p. 89-96.

Tang, H., Eronen, J. T., Micheels, A., and Fortelius, M., 2011, Regional climate model experiment to investigate the Asian monsoon in the Late Miocene: Climate of the Past.

Tejada-Lara, J. V., MacFadden, B. J., Bermudez, L., Rojas, G., Salas-Gismondi, R., and Flynn, J. J., 2018, Body mass predicts isotope enrichment in herbivorous mammals: Proc. R. Soc. B, v. 285, no. 1881, p. 20181020.

Tieszen, L. L., Senyimba, M. M., Imbamba, S. K., and Troughton, J. H., 1979, The distribution of C3 and C4 grasses and carbon isotope discrimination along an altitudinal and moisture gradient in Kenya: Oecologia, v. 37, no. 3, p. 337-350.

Tipple, B., Meyers, S., and Pagani, M., 2010, Carbon isotope ratio of Cenozoic CO2: A comparative evaluation of available geochemical proxies: Paleoceanography, v. 25, no. 3, p. 11.

Uno, K. T., Cerling, T. E., Harris, J. M., Kunimatsu, Y., Leakey, M. G., Nakatsukasa, M., and Nakaya, H., 2011, Late Miocene to Pliocene carbon isotope record of differential diet change among East African herbivores: Proceedings of the National Academy of Sciences, v. 108, no. 16, p. 6509-6514.

Uno, K. T., Polissar, P. J., Jackson, K. E., and deMenocal, P. B., 2016a, Neogene biomarker record of vegetation change in eastern Africa: Proceedings of the National Academy of Sciences of the United States of America, v. 113, no. 23, p. 6355-6363.

Uno, K. T., Polissar, P. J., Kahle, E., Feibel, C., Harmand, S., Roche, H., and deMenocal, P. B., 2016b, A Pleistocene palaeovegetation record from plant wax biomarkers from the Nachukui Formation, West Turkana, Kenya: Phil. Trans. R. Soc. B, v. 371, no. 1698, p. 10.

Whybrow, P. J., Friend, P., Ditchfield, P., and Bristow, C. S., 1999, Local stratigraphy of the Neogene outcrops of the coastal area:Western Region, Emiarate of Abu Dhabi, United Arab Emirates, *in* Whybrow, P. J., and Hill, A., eds., Fossil Vertebrates of Arabia: New Haven, Connecticut, Yale University Press,, p. 28-37.

Whybrow, P. J., and Hill, A., 1999, Fossil Vertebrates of Arabia: New Haven, Connecticut, Yale University Press, p. 523.

Young, H. J., and Young, T. P., 1983, Local Distribution of C_3 and C_4 Grasses in Sites of Overlap on Mount Kenya: Oecologia, v. 58, no. 3, p. 373-377.

Zazzo, A., Bendrey, R., Vella, D., Moloney, A., Monahan, F., and Schmidt, O., 2012, A refined sampling strategy for intra-tooth stable isotope analysis of mammalian enamel: Geochimica et Cosmochimica Acta, p. 13.

Zhang, Z., Ramstein, G., Schuster, M., Li, C., Contoux, C., and Yan, Q., 2014, Aridification of the Sahara desert caused by Tethys Sea shrinkage during the Late Miocene: Nature, v. 513, no. 7518, p. 401-404.

Zhuang, G., Pagani, M., and Zhang, Y. G., 2017, Monsoonal upwelling in the western Arabian Sea since the middle Miocene: Geology, v. 45, no. 7, p. 655-658.

TABLES

Table 18.1. Calculated δ13C values (‰, VPDB) for plant waxes, paleosol carbonate, enamel, and formed in equilibrium with C3 and C4 vegetation. The atmospheric CO2 value is from the high resolution benthic foramanifera record in Tipple et al. (2010). Enrichement factors for CO2-plants and for diet-enamel are from Cerling and Harris (1999); for n-alkanes, from Collister et al (1994); and for pedogenic carbonates, from Cerling (1984).

	$\delta^{13}C$ atmos.	εCO_2-C_3plant	$\delta^{13}C$ plant	$\delta^{13}C$ plant	εCO_2-C_4plant	$\delta^{13}C$ plant	εplant-proxy	**$\delta^{13}C$**	**$\delta^{13}C$**	**$\delta^{13}C$**
substrate	CO_2		avg. C_3	max. C_3		C_4		**avg. C3**	**max. C3**	**avg C_4**
n-alkanes	-6.3	19.6	-25.4	-22.6	4.7	-10.9	-8.0	-33.1	-30.3	-18.8
fossil enamel	-6.3	19.6	-25.4	-22.6	4.7	-10.9	+14.1	-11.4	-8.6	3.2
pedeogenic carbonate	-6.3	19.6	-25.4	-22.6	4.7	-10.9	+14	-11.4	-8.7	3.1

Table 18.2. n-Alkane sample information, concentration data, and CPI and ACL values.

								***n*-alkane concentration (ng/g sediment)**								
Lab ID	**Sample ID1**	**Sample ID2**	**Site**	**Lithology**	**sample mass (g)**	**CPI**	**ACL**	**nC 27**	**nC2 8**	**nC2 9**	**nC3 0**	**nC3 1**	**nC3 2**	**nC3 3**	**nC3 4**	**nC35**
KU369_F1	AD14.H 5.111B	Hamra 5.1	HMR 5	green clayey silt	118.8	3.1	30.1	50.7	24.2	50.4	20.2	64.6	11.2	37.2	3.7	10.4
KU370_F1	AD14.H 5.109B	Hamra 5.2	HMR 5	brown clayey silt	131.3	6.7	30.3	4.9	1.9	8.7	1.6	12.6	0.9	6.3	0.2	0.6
KU375_F1	5H42 IIaria #3	Hamra 5.3	HMR 5	green clayey silt	103.2	3.3	29.6	4.7	1.9	4.3	1.2	4.2	0.7	1.8	0.2	0.4
KU371_F1	AD14.K H.107B	Kihal 107	KIH 2	green clayey silt	124.3	3.3	29.7	4.7	1.9	4.0	1.2	4.2	0.6	2.0	0.2	0.6
KU372_F1	AD14.K H.108B	Kihal 108	KIH 2	green clayey silt	118.5	4.4	29.6	4.9	1.8	5.2	1.1	5.4	0.5	2.1	0.1	0.2
KU373_F1	AD14. M1.101 B	Mleisa 1	MLS 1	trackwayla yer silt	126.2	3.6	28.8	4.3	1.2	2.7	0.6	1.8	0.1	0.6	0.1	0.2
KU374_F1	AD14.R U.112B	Ruwais	RUW SE	brown silty clay	111.2	5.2	30.5	2.5	1.0	3.2	0.7	4.6	0.4	2.9	0.3	0.7
								***n*-alkanoic acid concentration (ng/g sediment)**								

								nC26	nC27	nC28	nC29	nC30	nC31	nC32	nC33	nC34
KU369_F3 AMeF3	AD14.H 5.111B	Hamra 5.1	HMR 5	green clayey silt	118.8	2.2	27.6	27.8	112.1	190.1	45.4	60.9	17.3	24.9	4.1	6.1
KU370_F3 AMeF3	AD14.H 5.109B	Hamra 5.2	HMR 5	brown clayey silt	131.3	2.6	27.9	17.4	8.2	19.5	5.4	9.0	1.8	3.1	0.2	0.3
KU375_F3 AMeF3	5H42 IIaria #3	Hamra 5.3	HMR 5	green clayey silt	103.2	2.6	27.6	23.3	95.5	203.9	39.0	66.0	15.1	21.7	3.6	5.1
KU371_F3 AMeF3	AD14.K H.107B	Kihal 107	KIH 2	green clayey silt	124.3	2.4	28.0	5.8	3.6	8.2	1.8	2.8	0.7	1.1	0.1	0.2
KU372_F3 AMeF3	AD14.K H.108B	Kihal 108	KIH 2	green clayey silt	118.5	2.5	27.5	6.9	3.6	7.8	1.3	1.6	0.4	0.4	0.1	0.1
KU373_F3 AMeF3	AD14. M1.101 B	Mleisa 1	MLS 1	trackwayla yer silt	126.2	2.5	27.0	5.7	2.0	3.1	0.5	0.6	0.2	0.1	0.0	0.0
KU374_F3 AMeF3	AD14.R U.112B	Ruwais	RUW SE	brown silty clay	111.2	2.6	27.2	2.2	0.8	1.4	0.3	0.4	0.1	0.1	0.0	0.0

Table 18.3. Carbon isotope data (‰, VPDB) for odd-chain n-alkanes (C27 to C35) and even-chain fatty acids (C26 to C34). Percent C4 vegetation is calculated from the *n*-C31alkane where uncertainty, given as 1σ accounts for C3 and C4 endmember variability and analytical uncertainty.

				***n*-alkane δ¹³C**							(WGS 84)	
Lab ID	**Sample ID1**	**Sample ID2**	**Site**	**C27**	**C29**	**C31**	**C33**	**C35**	**%C4**	**± %C4**	**lat (north)**	**long (east)**
KU369_F1	AD14.H5.111B	Hamra 5.1	HMR 5	-27.4	-26.5	-25.7	-25.2	-23.5	52	13	24.10309	52.52832
KU370_F1	AD14.H5.109B	Hamra 5.2	HMR 5	-26.7	-27.0	-28.0	-26.9	-25.5	36	15	24.103	52.528
KU375_F1	5H42 IIaria #3	Hamra 5.3	HMR 5	-28.0	-27.3	-27.2	-26.4	-24.7	41	14	24.103	52.528
KU371_F1	AD14.KH.107B	Kihal 107	KIH 2	-25.1	-26.0	-25.7	-25.3	-23.7	52	13	24.11847	53.02075
KU372_F1	AD14.KH.108B	Kihal 108	KIH 2	-26.0	-26.3	-26.9	-26.3	-25.4	43	13	24.11900	53.02004
KU373_F1	AD14.M1.101B	Mleisa 1	MLS 1	-22.0	-23.0	-22.6	-22.8	-23.1	73	12	23.94812	53.06154
KU374 F1	AD14.RU.112B	Ruwais	RUW SE	-27.2	-28.6	-29.2	-28.1	-26.4	27	16	24.07529	52.78897
			min	*-28.0*	*-28.6*	*-29.2*	*-28.1*	*-26.4*	*27*			
			max	*-22.0*	*-23.0*	*-22.6*	*-22.8*	*-23.1*	*73*			
			mean	*-26.1*	*-26.4*	*-26.5*	*-25.8*	*-24.6*	*46*			
			stdev	*2.0*	*1.7*	*2.1*	*1.7*	*1.2*	*15*			
			median	*-26.7*	*-26.5*	*-26.9*	*-26.3*	*-24.7*	*43*			

				***n*-alkanoic acid δ¹³C**								
Lab ID	**Sample ID1**	**Sample ID2**	**Site**	**C26**	**C28**	**C30**	**C32**	**C34**			**lat (north)**	**long (east)**
KU369_F3 AMeF2	AD14.H5.111B	Hamra 5.1	HMR 5	-29.2	-30.1	-28.5	-25.4	-28.5	--	--	24.10309	52.52832
KU370_F3 AMeF2	AD14.H5.109B	Hamra 5.2	HMR 5	-28.5	-29.8	-28.2	-25.8	-25.3	--	--	24.103	52.528
KU375_F3 AMeF2	5H42 IIaria #3	Hamra 5.3	HMR 5	-28.5	-30.6	-28.9	-27.7	-28.9	--	--	24.103	52.528
KU371_F3 AMeF2	AD14.KH.107B	Kihal 107	KIH 2	-25.7	-27.0	-26.3	-24.7	-24.8	--	--	24.11847	53.02075
KU372_F3 AMeF2	AD14.KH.108B	Kihal 108	KIH 2	-27.5	-28.8	-27.1	-24.3	-24.1	--	--	24.11900	53.02004
KU373_F3 AMeF2	AD14.M1.101B	Mleisa 1	MLS 1	-21.9	-23.2	-22.9	-21.5	-23.6	--	--	23.94812	53.06154
KU374_F3 AMeF2	AD14.RU.112B	Ruwais	RUW SE	-28.1	-29.1	-28.9	-28.3	-26.2	--	--	24.07529	52.78897
			min	*-29.2*	*-30.6*	*-28.9*	*-28.3*	*-28.9*				
			max	*-21.9*	*-23.2*	*-22.9*	*-21.5*	*-23.6*				
			mean	*-27.0*	*-28.4*	*-27.3*	*-25.4*	*-25.9*				
			stdev	*2.5*	*2.6*	*2.2*	*2.3*	*2.1*				
			median	*-28.1*	*-29.1*	*-28.2*	*-25.4*	*-25.3*				

Table 18.4. Comparison of tooth enamel carbon and oxygen isotope data (‰, VPDB) from treated and untreated samples. Treatment methods are described in the text.

Sample ID	**δ¹³C**				**δ¹⁸O**		
	UNT	**TRT**	**TRT-UNT**		**UNT**	**TRT**	**TRT-UNT**
AUH_1554-3	-0.1	-0.0	0.1		-3.6	-2.6	1.0
AUH_1554-6	0.2	-0.0	-0.2		-3.9	-3.1	0.8
AUH_1554-24	-1.4	-1.3	0.1		-2.0	-1.0	1.0
AUH_1554-27	-2.3	-2.0	0.3		-2.1	-1.3	0.7
AUH_1554-30	-1.9	-2.2	-0.3		-2.9	-1.9	0.9
AUH_1554-48	-0.8	-0.6	0.2		-5.6	-5.9	-0.3
AUH_1554-51	-0.3	-0.5	-0.2		-5.7	-6.0	-0.3
AUH_1554-54	-0.6	-0.6	-0.1		-4.1	-4.5	-0.4
AUH-1295-6	-6.4	-5.8	0.6		-3.7	-4.0	-0.3
AUH-1295-9	-6.6	-6.4	0.3		-3.6	-5.5	-1.9
AUH-1295-12	-4.4	-5.0	-0.6		-2.2	-4.6	-2.4
		avg	***0.0***				***-0.1***
		stdev	***0.3***				***1.2***

		min	***-0.6***				***-2.4***
		max	***0.6***				***1.0***

Table 18.5. Tooth enamel carbon and oxygen isotope data for Baynunah large mammals (‰,VPDB). Percent C4 diet is given along with uncertainty (1σ) that accounts for C3 and C4 endmember variability and analytical uncertainty. Data in this table includes carbon and oxygen values from Kingston, 1999. The original oxygen isotope values from Kingston are also provided (K99). [TYPESETTER - THIS TABLE IN LANDSCAPE ORIENTATION]

										K99	
Specimen ID	**Other ID**	**Family**	**Taxon**	**Element**	**Site**	**%C4**	**± %C4**	**$\delta^{13}C$**	**$\delta^{18}O$**	**$\delta^{18}O$**	**Source**
AUH 266		Bovidae	*Pachyportax latidens*	lt. m2	HMR 6	51	12	-4.0	-2.9	--	this study
AUH 278		Bovidae	*Pachyportax latidens*	lt. molar frag.	HMR 5	79	12	0.1	-2.3	-4.6	Kingston, 1999
AUH 27	AD 628	Bovidae	*Tragoportax cyrenaicus*	fragment	SHU 1	36	14	-6.1	0.4	-2.0	Kingston, 1999
AUH 239		Bovidae	*Tragoportax cyrenaicus*	molar frag.	THM 1	7	19	-10.4	-0.3	-2.6	Kingston, 1999
AD635		Bovidae	*Gen* et *sp* indet.	molar frag.	THM 1	33	15	-6.6	-3.7	-6.0	Kingston, 1999
AUH 1124		Giraffidae	*Gen* et *sp* indet.	molar frag.	RDB 1-1	73	12	-0.8	8.2	--	this study
AUH 204 avg.		Giraffidae	?*Bramatherium* sp.	rt. M frag.	RDB 2	79	12	0.2	8.5	--	this study
AUH 206 avg.	1165	Giraffidae	?*Bramatherium* sp.	unworn M frag.	RDB 2	68	12	-1.5	4.9	0.2	this study; Kingston, 1999
AUH 211	AD 627a	Giraffidae	cf. *Samotherium* or *Palaeotragus germaini*	lt. M frag	RDB 2	15	18	-9.2	6.6	4.3	Kingston, 1999
AUH 372	AD 766	Giraffidae	?*Bramatherium* sp.	lt. M	RDB 2	40	14	-5.6	-2.6	-4.9	Kingston, 1999
AUH 217	AD 767	Giraffidae	?*Bramatherium* sp.	rt. dP4	RDB 2	60	12	-2.7	4.3	1.9	Kingston, 1999

AUH 29		Hippopotamidae	*Archaeopotamus* cf. *qeshta*	canine	SHU 1	78	12	0.0	-4.7	--	this study
AUH 31		Hippopotamidae	*Gen* et *sp* indet.	molar	SHU 1	77	12	-0.2	-4.0	--	this study
AUH 60		Hippopotamidae	*Gen* et *sp* indet.	premolar	SHU 1	73	12	-0.8	-6.5	--	this study
AUH 92		Hippopotamidae	*Gen* et *sp* indet.	premolar	SHU 1	68	12	-1.5	-3.3	--	this study
AUH 110		Hippopotamidae	*Archaeopotamus* cf. *qeshta*	lt. m2	SHU 1	77	12	-0.2	-4.6	--	this study
AUH 359		Hippopotamidae	*Archaeopotamus qeshta*	canine frag.	HAR 1	80	12	0.3	-3.6	--	this study
AUH 421		Hippopotamidae	*Archaeopotamus qeshta*	P4	JDH 4	70	12	-1.2	-5.9	--	this study
AD 630		Hippopotamidae	*Gen* et *sp* indet.	molar frag.	JDH	76	12	-0.3	-8.2	-10.5	Kingston, 1999
AD 631		Hippopotamidae	*Gen* et *sp* indet.	molar frag.	SHU 1	67	12	-1.7	-6.1	-8.4	Kingston, 1999
AUH 1728		Hippopotamidae	*Gen* et *sp* indet.	upper premolar	RUWC	67	12	-1.7	-7.1	--	this study
AUH 619a	BMNH-M49464	Hippopotamidae	*Archaeopotamus qeshta*	fragment	JBR 2	40	14	-5.5	-6.2	-8.5	Kingston, 1999
AUH 329		Suidae	*Nyanzachoerus syticus*	lt m3	HMR 1	2	20	-11.1	-0.7	--	this study
AUH 784		Suidae	*Nyanzachoerus syticus*	molar crown frag.	RDB 2	6	20	-10.6	-3.4	--	this study
AUH 55		Suidae	*Propotomochoerus hysudricus*	lt M3	SHU 1	12	18	-9.7	-3.2	--	this study
AUH 1295		Equidae	*Gen* et *sp* indet.	rt P4 or M1	HMR 5	70	12	-1.1	-2.6	--	this study
AUH 1465		Equidae	*Gen* et *sp* indet.	lower tooth	SHU 2	50	13	-4.1	-1.4	--	this study
AUH 1535		Equidae	*"Hipparion" abudhabiense*	lt m1 or m2	GAA 2	66	12	-1.7	-4.7	--	this study
AUH 1554		Equidae	*Gen* et *sp* indet.	rt. m1 or m2	GAA 1	72	12	-0.8	-3.1	--	this study

AUH 1566		Equidae	*Gen* et *sp* indet.	rt. M1 or M2	GAA 3	49	13	-4.3	-4.5	--	this study
AUH 1712		Equidae	*"Hipparion" abudhabiense*	p4 or m1	JBR	47	13	-4.5	-1.6	--	this study
AUH 609	AD 621	Equidae	"Hipparion" sp.	fragment	JDH 3	65	12	-1.9	-3.8	-6.1	Kingston, 1999
AUH 46	AD 622a	Equidae	"Hipparion" sp.	fragment	HMR 5	53	12	-3.6	-4.3	-6.6	Kingston, 1999
AUH 23	AD 623	Equidae	*"Hipparion" abudhabiense*	lt molar frag.	SHU 1	37	14	-6.1	-3.5	-5.9	Kingston, 1999
AD 633		Equidae	"Hipparion" sp.	molar frag.	KIH	82	12	0.5	-2.8	-5.1	Kingston, 1999
AD 634		Equidae	"Hipparion" sp.	molar frag.	HMR 5	40	14	-5.6	-1.6	-4.0	Kingston, 1999
AUH 208	AD 750	Equidae	"Hipparion" sp.	lower molar frag.	RDB 2	24	16	-7.8	-0.4	-2.7	Kingston, 1999
AUH 231a	AD 751	Equidae	*"Hipparion" abudhabiense*	P3 or P4	HMR 5	72	12	-1.0	-5.9	-8.3	Kingston, 1999
AUH 260	AD 752	Equidae	*"Hipparion" abudhabiense*	upper ? molar	KIH 1	62	12	-2.4	-4.4	-6.7	Kingston, 1999
AUH 212	AD 753	Equidae	"Hipparion" sp.	m1 or m2	RDB 2	75	12	-0.4	1.8	-0.5	Kingston, 1999
AUH 178	AD 754	Equidae	"Hipparion" sp.	rt. P3 or P4	JDH 5	55	12	-3.3	-1.5	-3.8	Kingston, 1999
AUH 205	AD 757	Equidae	"Hipparion" sp.	rt. P3 or P4	RDB 2	28	15	-7.4	1.7	-0.6	Kingston, 1999
AUH 115	AD 758	Equidae	*"Hipparion" abudhabiense*	M1 or M2	SHU 1	76	12	-0.3	-4.4	-6.8	Kingston, 1999
AD 759	M50664	Equidae	"Hipparion" sp.	P2	JBR 2	78	12	0.0	-4.4	-6.8	Kingston, 1999
AD 760	M50663	Equidae	*"Hipparion" abudhabiense*	rt lower molar	JBR 2	84	12	0.9	-0.8	-3.1	Kingston, 1999
AUH 174	AD 761	Equidae	*"Hipparion" abudhabiense*	rt lower premolar	HMR 1	73	12	-0.7	-4.0	-6.4	Kingston, 1999
AUH 72	AD 763	Equidae	*"Hipparion" abudhabiense*	lower molar	SHU 1	54	12	-3.5	-4.7	-7.0	Kingston, 1999

AUH 265	AD 764	Equidae	"Hipparion" sp.	rt lower premolar	JDH 4	69	12	-1.4	-2.3	-4.7	Kingston, 1999
AUH 677	AD 765	Equidae	*Gen* et *sp* indet.	rt lower molar	SHU 4	35	14	-6.3	-4.9	-7.3	Kingston, 1999
AUH 162		Rhinocerotidae	*Gen* et *sp* indet.	fragment	SHU 1	9	19	-10.2	-3.9	--	this study
AUH 43		Rhinocerotidae	*Gen* et *sp* indet.	fragment	SHU 1	7	19	-10.4	-3.7	--	this study
AUH 159		Deinotheriidae	aff. *Deinotherium bozasi*	molar frag.	SHU 1	0	22	-12.4	-0.2	--	this study
AUH 21		Deinotheriidae	aff. *Deinotherium bozasi*	molar frag.	SHU 1	0	23	-13.2	-3.0	--	this study
AUH 10		Elephantidae	*Stegatetrabelodon emiratus*	molar frag.	HMR 2	63	12	-2.2	-2.9	--	this study
AUH 10-W		Elephantidae	*Stegatetrabelodon emiratus*	molar frag.	HMR 2	58	12	-3.0	-2.2	--	this study
AUH 1171		Elephantidae	*Stegatetrabelodon emiratus*	lt. M1 (juvenile)	HMR 3-1	71	12	-1.0	2.2	--	this study
AUH 168		Elephantidae	*Stegatetrabelodon emiratus*	molar frag.	SHU 1	37	14	-6.0	-0.2	--	this study
AUH 233 avg.	1163; 632?	Elephantidae	*Stegatetrabelodon emiratus*	molar frag.	HMR 6	69	12	-1.3	-2.3	-4.7	this study; Kingston, 1999
AUH 234		Elephantidae	*Stegatetrabelodon emiratus*	M2? frag.	SHU 4	77	12	-0.2	0.2	--	this study
AUH 373		Elephantidae	*Stegatetrabelodon emiratus*	molar frag.	HMR 3	72	12	-0.9	-2.5	--	this study
AUH 456		Elephantidae	*Stegatetrabelodon emiratus*	rt. m3	RDB 2	28	15	-7.3	-2.1	--	this study
AUH 672		Elephantidae	*Stegatetrabelodon emiratus*	molar frag.	MIM 1	68	12	-1.4	-2.1	--	this study
AD 629		Elephantidae	*Stegatetrabelodon emiratus*	molar frag.	JBR east	47	13	-4.5	-4.2	-6.5	Kingston, 1999
AD 632		Elephantidae	*Stegatetrabelodon emiratus*	molar frag.	HMR	65	12	-2.0	-3.0	-5.3	Kingston, 1999

BSPG 1965 I112 avg		Gomphotheriidae	*Gen* et *sp* indet.	lt. m3	JBR	48	13	-4.3	-1.1	--	this study

Table 18.6. Intratooth stable isotope (‰, VPDB) and %C4 (± 1σ) data for Equidae molar profiles. Smoothed data (3 pt., weighted 0.25/0.50/0.25) and inverse model results (estimated input signal) are given with 2σ uncertainty. Sample locations are given as distance from the cervix. Summary statistics are provided for each intratooth profile. Estimated input signal was calculated using Matlab code modified from "mSolve_1.m" published by Passey et al. (2005).

	measured (smoothed)		**estimated input signal (model results)**						**distance**
Sample ID	**$\delta^{13}C$**	**$\delta^{18}O$**	**$\delta^{13}C$**	**±2σ $\delta^{13}C$**	**$\delta^{18}O$**	**±2σ $\delta^{18}O$**	**%C4**	**±1σ %C4**	**(mm)**
AUH-1554-3	-0.0	-2.6	-1.2	0.6	-4.1	1.2	70	12	3
AUH-1554-6	-0.0	-3.1	-0.2	0.6	-4.7	1.2	76	12	6
AUH-1554-9	0.4	-2.2	1.4	0.8	-3.8	0.8	87	12	9
AUH-1554-12	0.5	-2.1	2.5	1.0	-4.2	0.7	95	13	12
AUH-1554-15	0.4	-1.8	2.7	1.0	-3.5	0.8	97	13	15
AUH-1554-18	-0.4	-1.4	1.0	1.0	-2.8	0.8	85	12	18
AUH-1554-21	-1.3	-1.5	0.2	0.6	-1.2	1.3	79	12	21
AUH-1554-24	-1.3	-1.0	-0.3	0.9	0.6	1.3	76	12	24
AUH-1554-27	-2.0	-1.3	-1.7	0.8	0.5	1.4	66	12	27
AUH-1554-30	-2.2	-1.9	-2.1	0.7	-0.1	1.4	64	12	30
AUH-1554-33	-2.0	-2.9	-1.6	0.6	-1.1	1.2	67	12	33
AUH-1554-36	-1.7	-3.7	-2.0	0.8	-1.2	0.9	64	12	36
AUH-1554-39	-1.8	-4.0	-2.8	0.6	-1.4	1.1	59	12	39
AUH-1554-42	-1.4	-4.7	-2.2	0.8	-2.9	0.9	63	12	42
AUH-1554-45	-0.8	-5.3	-1.7	0.5	-4.6	1.2	66	12	45
AUH-1554-48	-0.6	-5.9	-1.6	0.5	-6.0	1.4	67	12	48
AUH-1554-51	-0.5	-6.0	-1.8	0.8	-5.3	1.9	66	12	51
AUH-1554-54	-0.6	-4.5	-1.7	0.7	-4.4	1.2	67	12	54
AUH-1554-CEM	-3.4	-4.1	--	--	--	--	--	--	--
min	*-2.2*	*-6.0*	*-2.8*	--	*-6.0*	--	*59*		
max	*0.5*	*-1.0*	*2.7*	--	*0.6*	--	*97*		
range	*2.7*	*5.0*	*5.5*	--	*6.6*	--	*38*		

mean	*-0.8*	*-3.1*	*-0.7*	--	*-2.8*	--	*73*		
AUH-1295-3	-2.8	0.2	-4.7	0.8	4.4	2.8	46	13	3
AUH-1295-6	-2.8	-2.1	-4.4	0.9	-1.1	1.8	48	13	6
AUH-1295-9	-2.1	-2.9	-3.6	0.8	-1.5	1.3	53	12	9
AUH-1295-12	-1.6	-3.4	-2.9	0.8	-4.0	1.9	58	12	12
AUH-1295-15	-0.9	-4.4	-2.1	0.6	-6.2	1.3	64	12	15
AUH-1295-18	-0.6	-3.9	-1.4	0.6	-4.6	1.4	68	12	18
AUH-1295-21	-0.3	-3.1	-0.6	0.7	-3.4	1.1	74	12	21
AUH-1295-24	-0.0	-2.5	0.2	0.9	-3.6	0.8	79	12	24
AUH-1295-27	-0.1	-2.5	0.3	1.0	-3.5	1.7	80	12	27
AUH-1295-30	-0.3	-1.8	-1.0	1.5	-1.5	2.8	71	12	30
AUH-1295-33	-1.5	-0.9	-1.3	0.8	-1.7	2.0	69	12	33
AUH-1295-CEM	-3.5	-3.8	--	--	--	--	--	--	--
min	*-2.8*	*-4.4*	*-4.7*	--	*-6.2*	--	*46*		
max	*-0.0*	*0.2*	*0.3*	--	*4.4*	--	*80*		
range	*2.8*	*4.6*	*4.9*	--	*10.6*	--	*34*		
mean	*-1.2*	*-2.5*	*-2.0*	--	*-2.4*	--	*65*		
AUH-1566-3	-6.8	-0.8	-5.9	1.0	2.1	2.2	38	14	3
AUH-1566-6	-6.8	-0.8	-7.2	1.1	2.8	2.2	29	15	6
AUH-1566-9	-7.1	-2.1	-8.2	0.9	1.7	1.9	22	16	9
AUH-1566-12	-6.5	-3.0	-7.5	1.0	0.4	1.8	27	16	12
AUH-1566-15	-5.5	-4.5	-7.5	0.8	-2.4	1.9	27	16	15
AUH-1566-18	-5.4	-5.9	-7.8	0.9	-3.3	0.9	25	16	18
AUH-1566-21	-4.6	-5.6	-6.9	0.9	-4.1	1.7	31	15	21
AUH-1566-24	-3.9	-6.8	-6.1	0.9	-6.8	1.3	37	14	24
AUH-1566-27	-3.2	-6.8	-5.4	0.6	-6.4	1.2	41	14	27
AUH-1566-30	-2.8	-6.1	-4.0	0.8	-6.0	1.2	51	12	30
AUH-1566-33	-2.0	-5.6	-2.8	0.7	-6.8	1.0	59	12	33
AUH-1566-36	-2.2	-5.4	-2.2	0.7	-6.7	1.2	63	12	36
AUH-1566-39	-2.1	-4.5	-1.9	0.6	-6.2	0.9	65	12	39
AUH-1566-42	-2.5	-4.6	-2.3	1.3	-7.1	1.6	62	12	42
AUH-1566-45	-2.8	-4.5	-2.2	1.2	-6.5	1.3	63	12	45
AUH-1566-CEM	-5.6	-4.2	--	--	--	--	--	--	--

min	*-7.1*	*-6.8*	*-8.2*	--	*-7.1*	--	*22*		
max	*-2.0*	*-0.8*	*-1.9*	--	*2.8*	--	*65*		
range	*5.0*	*6.1*	*6.3*	--	*9.8*	--	*43*		
mean	*-4.3*	*-4.5*	*-5.2*	--	*-3.7*	--	*43*		
AUH-1535-6	-3.6	-2.8	-4.4	1.1	-1.3	1.0	48	13	6
AUH-1535-9	-3.3	-2.9	-4.8	1.2	-1.0	1.4	46	13	9
AUH-1535-12	-2.9	-3.4	-4.5	1.0	-1.0	1.4	47	13	12
AUH-1535-15	-2.3	-4.0	-4.4	0.8	-2.5	1.3	48	13	15
AUH-1535-18	-2.0	-5.3	-4.1	1.0	-4.1	0.8	50	13	18
AUH-1535-21	-1.3	-5.8	-3.3	0.8	-5.0	0.8	55	12	21
AUH-1535-24	-0.7	-6.2	-2.0	1.2	-5.5	0.7	64	12	24
AUH-1535-27	0.1	-6.2	-0.1	1.6	-5.3	1.0	78	12	27
AUH-1535-30	0.7	-6.0	0.1	1.5	-5.1	1.0	78	12	30
AUH-1535-CEM	-3.4	-4.4	--	--	--	--	--	--	--
min	*-3.6*	*-6.2*	*-4.8*	--	*-5.5*	--	*46*		
max	*0.7*	*-2.8*	*0.1*	--	*-1.0*	--	*78*		
range	*4.3*	*3.4*	*4.8*	--	*4.5*	--	*33*		
mean	*-1.7*	*-4.7*	*-3.0*	--	*-3.4*	--	*57*		
AUH-1465-3	-5.1	-0.4	-7.8	1.5	-0.6	1.0	25	16	3
AUH-1465-6	-4.0	-1.2	-5.9	0.9	-2.1	1.0	38	14	6
AUH-1465-9	-3.6	-1.3	-4.2	1.2	-2.6	1.4	49	13	9
AUH-1465-12	-2.6	-2.0	-2.6	0.8	-5.0	1.5	60	12	12
AUH-1465-15	-3.0	-2.5	-3.3	0.7	-3.7	1.8	56	12	15
AUH-1465-18	-3.1	-0.6	-2.7	0.7	0.1	1.4	59	12	18
AUH-1465-21	-3.1	0.2	-1.8	0.9	1.0	1.2	66	12	21
AUH-1465-24	-3.1	0.0	-1.9	0.9	2.5	1.6	65	12	24
AUH-1465-27	-3.8	0.4	-3.0	0.8	3.0	1.8	58	12	27
AUH-1465-30	-4.3	-0.9	-3.2	0.8	-0.2	1.8	56	12	30
AUH-1465-33	-4.8	-2.4	-3.7	0.8	-3.3	1.7	53	12	33
AUH-1465-36	-5.0	-3.1	-3.2	0.8	-5.6	2.9	56	12	36
AUH-1465-39	-4.8	-3.9	-5.0	1.5	-3.2	3.2	44	13	39
AUH-1465-42	-5.8	-0.8	-5.6	1.4	1.8	1.6	40	14	42
AUH-1465-45	-4.7	-1.3	-3.8	0.8	-0.1	1.1	52	12	45
min	*-5.8*	*-3.9*	*-7.8*	--	*-5.6*	--	*25*		

max	*-2.6*	*0.4*	*-1.8*	--	*3.0*	--	*66*		
range	*3.1*	*4.2*	*6.0*	--	*8.6*	--	*41*		
mean	*-4.1*	*-1.3*	*-3.8*	--	*-1.2*	--	*52*		
AUH-1712-3	-4.7	-3.4	-3.5	0.7	-3.5	1.7	54	12	3
AUH-1712-6	-4.6	-2.2	-3.2	0.7	1.0	2.0	56	12	6
AUH-1712-9	-4.8	-1.0	-4.2	0.9	1.7	1.6	49	13	9
AUH-1712-12	-5.6	-2.1	-6.4	0.9	-1.8	1.5	34	14	12
AUH-1712-15	-6.1	-3.4	-7.0	1.0	-2.5	0.8	30	15	15
AUH-1712-18	-5.6	-2.7	-6.3	0.7	-1.2	0.6	35	14	18
AUH-1712-21	-5.0	-2.7	-5.7	0.6	-2.8	1.3	39	14	21
AUH-1712-24	-4.6	-3.3	-4.8	0.7	-5.7	1.6	45	13	24
AUH-1712-27	-4.0	-3.9	-4.1	0.6	-6.6	1.7	50	13	27
AUH-1712-30	-3.9	-2.8	-4.4	0.5	-4.6	1.5	48	13	30
AUH-1712-33	-4.2	-1.7	-5.2	0.6	-3.3	1.5	43	13	33
AUH-1712-36	-4.3	-0.7	-5.2	0.5	-0.8	2.4	43	13	36
AUH-1712-39	-4.0	1.1	-4.6	0.6	0.2	1.6	46	13	39
AUH-1712-42	-4.0	-0.2	-4.4	0.6	-2.5	0.9	48	13	42
AUH-1712-45	-4.1	-0.6	-3.6	0.9	-1.6	1.3	53	12	45
AUH-1712-48	-3.6	0.2	-2.8	0.7	-0.6	1.1	59	12	48
AUH-1712-CEM	-5.3	-4.7	--	--	--	--	--	--	--
min	*-6.1*	*-3.9*	*-7.0*	--	*-6.6*	--	*30*		
max	*-3.6*	*1.1*	*-2.8*	--	*1.7*	--	*59*		
range	*2.5*	*5.0*	*4.1*	--	*8.3*	--	*28*		
mean	*-4.6*	*-1.8*	*-4.7*	--	*-2.2*	--	*46*		

Table 18.7. Modern δ18O values for precipitation include measured values from the United Arab Emirates (UAE) and the GNIP station from Bahrain (n=102; 2σ) and modeled values for western Abu Dhabi based on the Online Isotopes in Precipiation Calculator (OIPC; 95% CI).

Precipitation Location	$\delta^{18}O$	δD
Bahrain Airport (GNIP Station)	+0.5 ± 5.6	+12.4 ± 35
UAE (Rizk and Alhsharhan, 2003)	+0.8	+12.4
OIPC (Bowen, 2019)	+0.1 ± 0.4	+12.4 ± 17.3
average	***+0.5***	***+12.4***

Table 18.8. Summary statistics of percent C4 vegetation and diet at different Baynunah Formation fossil sites. Median uncertainty in percent C4 calculations is ±12%.

			Percent C4		
Site		**diet**	***n*-alkane**	**ped carb**	
Hamra		2	36	16	min.
		79	52	63	max.
		65	41	37	median
		13	3	9	n
Kihal		62	43	45	min.
		82	52	62	max.
		72	47	53	median
		2	2	2	n
Jebel Baraka		40	--	32	min.
		84	--	55	max.
		48	--	45	median
		6	--	3	n
Shuwaihat		0	--	--	min.
		78	--	--	max.
		50	--	48	median
		19	--	1	n
Ruwais		67	27	--	
		1	1	--	n
All data		0	27	16	min.
		84	73	63	max.
		63	43	40	median
		24	15	15	1σ
		84	46	47	range
		65	7	15	n

Table 18.9. Fraction woody cover (fwc) data calculated from pedogenic carbonate δ13C values from Baynunah, Lothagam, and the Pakistani Siwaliks. Data from the latter two sites are restricted to 8 to 6 Ma and all paleomagnetic based ages for the Siwaliks were updated to the timescale of Gradstein and Ogg (2012). Data are from Kingston (1999), Cerling et al. (2003a), Quade et al. (1989), and Behrensmeyer et al. (2007).

		Percent of data set by site		
fwc	**Ecosystem type**	**Baynunah**	**Lothagam**	**Siwaliks**
>0.4	*grassy woodland, bushland or shrubland to forest*	*26%*	*24%*	*73%*
0.4 to 0.1	*woody grassland*	*69%*	*70%*	*24%*
>0.1	*grassland*	*5%*	*6%*	*3%*